



HAL
open science

The Limpopo Magma-Rich Transform Margin, South Mozambique: 1. Insights From Deep-Structure Seismic Imaging

L. Watremez, S. Leroy, E. d'Acremont, V. Roche, M. Evain, A. Leprêtre, F. Verrier, D. Aslanian, N. Dias, A. Afilhado, et al.

► **To cite this version:**

L. Watremez, S. Leroy, E. d'Acremont, V. Roche, M. Evain, et al.. The Limpopo Magma-Rich Transform Margin, South Mozambique: 1. Insights From Deep-Structure Seismic Imaging. *Tectonics*, 2021, 40, 10.1029/2021TC006915 . insu-03594270

HAL Id: insu-03594270

<https://insu.hal.science/insu-03594270>

Submitted on 24 Jun 2022

HAL is a multi-disciplinary open access archive for the deposit and dissemination of scientific research documents, whether they are published or not. The documents may come from teaching and research institutions in France or abroad, or from public or private research centers.

L'archive ouverte pluridisciplinaire **HAL**, est destinée au dépôt et à la diffusion de documents scientifiques de niveau recherche, publiés ou non, émanant des établissements d'enseignement et de recherche français ou étrangers, des laboratoires publics ou privés.

Copyright

Tectonics®

RESEARCH ARTICLE

10.1029/2021TC006915

This article is a companion to Roche et al. (2021), <https://doi.org/10.1029/2021TC006914>

Key Points:

- New seismic velocity models across east Limpopo delineates crustal domains, from stretched continental crust to thick oceanic crust
- Intense magmatic activity associated with a mantle plume affected the entire margin during all stages of its formation
- Transform margin structure and geometry are controlled by structural inheritance, syn-tectonic sedimentation, and magmatic activity history

Supporting Information:

Supporting Information may be found in the online version of this article.

Correspondence to:

L. Watremez,
Louise.Watremez@univ-lille.fr



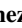
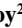




Citation:

Watremez, L., Leroy, S., d'Acremont, E., Roche, V., Evain, M., Leprêtre, A., et al. (2021). The Limpopo magma-rich transform margin, south Mozambique: 1. Insights from deep-structure seismic imaging. *Tectonics*, 40, e2021TC006915. <https://doi.org/10.1029/2021TC006915>

Received 21 MAY 2021

Accepted 15 NOV 2021

The Limpopo Magma-Rich Transform Margin, South Mozambique: 1. Insights From Deep-Structure Seismic Imaging

L. Watremez¹ , S. Leroy² , E. d'Acremont² , V. Roche² , M. Evain³ , A. Leprêtre³, F. Verrier³, D. Aslanian³ , N. Dias^{4,5} , A. Afilhado^{4,5}, P. Schnürle³, R. Castilla⁶, F. Despinois⁷, and M. Moulin³ 

¹Université de Lille, CNRS, Université Littoral Côte d'Opale, IRD, UMR 8187—LOG—Laboratoire d'Océanologie et de Géosciences, Lille, France, ²Sorbonne Université, CNRS, Institut des Sciences de la Terre de Paris, UMR 7193, ISTE, Paris, France, ³IFREMER, REM/GM/LGS, Centre de Brest, Plouzané, France, ⁴Instituto Dom Luis, Faculdade das Ciências, Universidade de Lisboa, Lisboa, Portugal, ⁵Instituto Superior de Engenharia de Lisboa, Instituto Politécnico de Lisboa, Lisboa, Portugal, ⁶Géo-Energie, Zürich, Switzerland, ⁷TotalEnergies SE, R&D Sustainability, Pau, France

Abstract A variety of structures results from the interplay of evolving far-field forces, plate kinematics, and magmatic activity during continental break-up. The east Limpopo transform margin, offshore northern Mozambique, formed as Africa and Antarctica separated during the mid-Jurassic period break-up of the Gondwana supercontinent. The nature of the crust onshore has been discussed for decades in an effort to resolve issues with plate kinematic models. Two seismic refraction profiles with coincident multichannel seismic reflection profiles allow us to interpret the seismic velocity structures across the margin, both onshore and offshore. These seismic profiles allow us to (a) delineate the major regional crustal domains; (b) identify widespread indications of magmatic activity; and (c) map crustal structure and geometry of this magma-rich transform margin. Careful examination of the profiles allows us to make the following observations and interpretations: (a) on land, continental crust is overlain by a >10-km thick volcano-sedimentary wedge related to an early rifting stage, (b) offshore, thick oceanic crust formed due to intense magmatic activity, and between the two (c) a 50–60-km wide transform zone where the crustal structures are affected by intense magmatic activity and faulting. The prominent presence of intrusive and extrusive igneous units may be attributed to the combination of a deep-seated melting anomaly and a trans-tensional fault zone running through thinned lithosphere that allowed melt to reach the surface. A comparison of the crustal thinning along other transform margins shows a probable dependence with the thermal and/or tectonic history of the lithosphere.

1. Introduction

The crustal structure of rifted continental margins can be highly variable (Blenkinsop & Moore, 2013) largely due to changes in plate kinematics during the sequential stages of rifting, break up, and ocean basin formation. Changes in plate motion during these stages can result in the segmentation of the rift and the subsequent spreading center, vertical movement of the crust, and affect the evolution of the thermal regime (Huisman & Beaumont, 2011). Thus, continental margins can be classified according to their orientation relative to the direction of plate motion: orthogonal being considered divergent margins, oblique being considered trans-tensional margins, and parallel being considered to transform margins. Changes in plate kinematics can induce an evolution from divergent to transform within the same margin (Brune et al., 2018; Philippon & Corti, 2016).

Transform margins are thought to develop through a series of stages: (a) the continent-continent stage of intra-continental transform faulting; (b) the continent-ocean shear stage in which the active transform margin develops; and (c) the post-shear stage of the passive transform margin (Ammann et al., 2018; Basile, 2015; Bird, 2001; Le Pichon & Hayes, 1971; Le Pourhiet et al., 2017; Lorenzo, 1997; Mascle & Blarez, 1987; Mercier de Lépinay et al., 2016). However, the tectonic and magmatic history of transform margins can be much more complex and variable than this simple classic model. Some transform margins exhibit evidence of at least one divergent episode prior to the development of transform motion (e.g., Guiana, Greenroyd et al., 2007; South-Africa; Hermann & Jokat, 2016; Demerara Plateau; Musser et al., 2021; Parsieglia et al., 2009; Jan Mayen Fracture Zone; Stankiewicz et al., 2008), or in some cases trans-tension, a combination of extension and shear (e.g., Edwards et al., 1997). Magmatic activity can occur at different stages of transform margin evolution: (a) during an early

divergent stage (e.g., Museur et al., 2021), (b) during transform motion resulting in a “leaky” transform (e.g., Greenroyd et al., 2008; Ritzmann et al., 2004), or (c) during all stages of transform margin evolution (e.g., Parsieglia et al., 2009). Thus, crustal structure and thermal evolution of transform margins can differ significantly from divergent margins (Mercier de Lépinay et al., 2016), and may result in such features as a marginal ridge and/or plateau (e.g., Basile, 2015; Basile et al., 1998; Loncke et al., 2020; Mercier de Lépinay et al., 2016; Nemčok et al., 2016; Sage et al., 2000).

Transform and divergent margins do exhibit some similarities in that their crustal structure can be categorized into three distinct domains: continental and oceanic, often with a transitional domain in between. These structural domains record the interplay of the tectonic and magmatic processes that formed them. The continental domain is characterized by unequivocal continental crust, showing a marked thinning in distal parts of the margin. The transitional domain corresponds to the transition from thinned continental crust to oceanic crust (e.g., Cannat et al., 2009; Jolivet et al., 2015; Nonn et al., 2017; Péron-Pinvidic & Manatschal, 2019; Péron-Pinvidic & Osmundsen, 2016; Sutra et al., 2013).

The continental rifted margins off the coast of Mozambique provide excellent examples of divergent, trans-tensional, and transform margins with significant structural and magmatic histories (Figure 1). Before this study, the nature and geometry of the distinct crustal domains were poorly known across segments of the Mozambique margin, in particular along the Mozambique Coastal Plain (Figure 1), and at transform margins in general due to the lack of high-resolution crustal-scale seismic data. Questions remained regarding the Early Jurassic igneous province that crops out around the Mozambique Coastal Plain (e.g., Melluso et al., 2008; Klausen, 2009) and is thought to be related to the Karoo mantle plume (e.g., Duncan et al., 1997; Svensen et al., 2012). Previous studies found onshore volcanic units and dyke complexes dating from ca. 183 Ma, potentially related to the rifting event (Duncan et al., 1997; Jourdan et al., 2006, 2007; Klausen, 2009), which may shed light on the early stages of margin development. While wide-angle and multi-channel seismic data from previous studies (Mahanjane, 2012; Leinweber et al., 2013; Mueller et al., 2016; Mueller & Jokat, 2017; Klimke et al., 2018; Senkans et al., 2019) have provided insights into the crustal structure of the Beira High and Angoche segments along the Central Mozambique margin, the tectonic structure, and nature of Mozambique's Limpopo margin crust are still poorly known (Figure 1). Remarkably, not only is the crustal structure of the offshore Limpopo unclear, but the nature of the onshore crust as far west as the Lebombo monocline and as far north as the MatakaSabi monocline (Leinweber & Jokat, 2011) is poorly constrained. It has been discussed as being either continental or oceanic based on gravity modeling showing that both interpretations are possible (Gwavava et al., 1992). Determining whether this region is continental or oceanic would have significant implications for conjugate margin studies and plate tectonic reconstructions.

Mapping carried out in this study reveals the margin crustal domains and improves our knowledge of the evolving magmatic supply during margin formation. Two seismic refraction profiles were acquired and analyzed in conjunction with existing industry seismic reflection profiles. We present the results of the velocity modeling and characterize the crustal domains of the Limpopo margin, providing a better understanding of the formation and evolution of this margin and perhaps that of conjugate margins in general.

This study is associated with that of Roche et al. (2021), which presents the structural interpretations with the identification of distinct tectonic deformation episodes.

2. Geological Setting

Several plate kinematic models based upon geological studies, potential field data, and seismic data propose reconstructed initial positions of Africa and Antarctica (Evain et al., 2021; Gaina et al., 2013; Klimke et al., 2018; Leinweber & Jokat, 2012; Reeves et al., 2016; Sahabi, 1993; Thompson et al., 2019). These plate kinematic models show that Africa and Antarctica were joined along what is now the Mozambique margin, before the break-up of Gondwana. The Africa-Antarctica Corridor (AAC), which separates the continental margin, is the result of the southward drift of Antarctica relative to Africa along the Davie and Mozambique fracture zones (Figure 1a). The Limpopo transform margin is located in the northwestern part of the AAC, between the African continent in the west and the deep-water Mozambique Basin in the east. It lies to the south of the magma-rich Beira High and Angoche divergent margin segments (Figures 1a and 1b; Senkans et al., 2019).

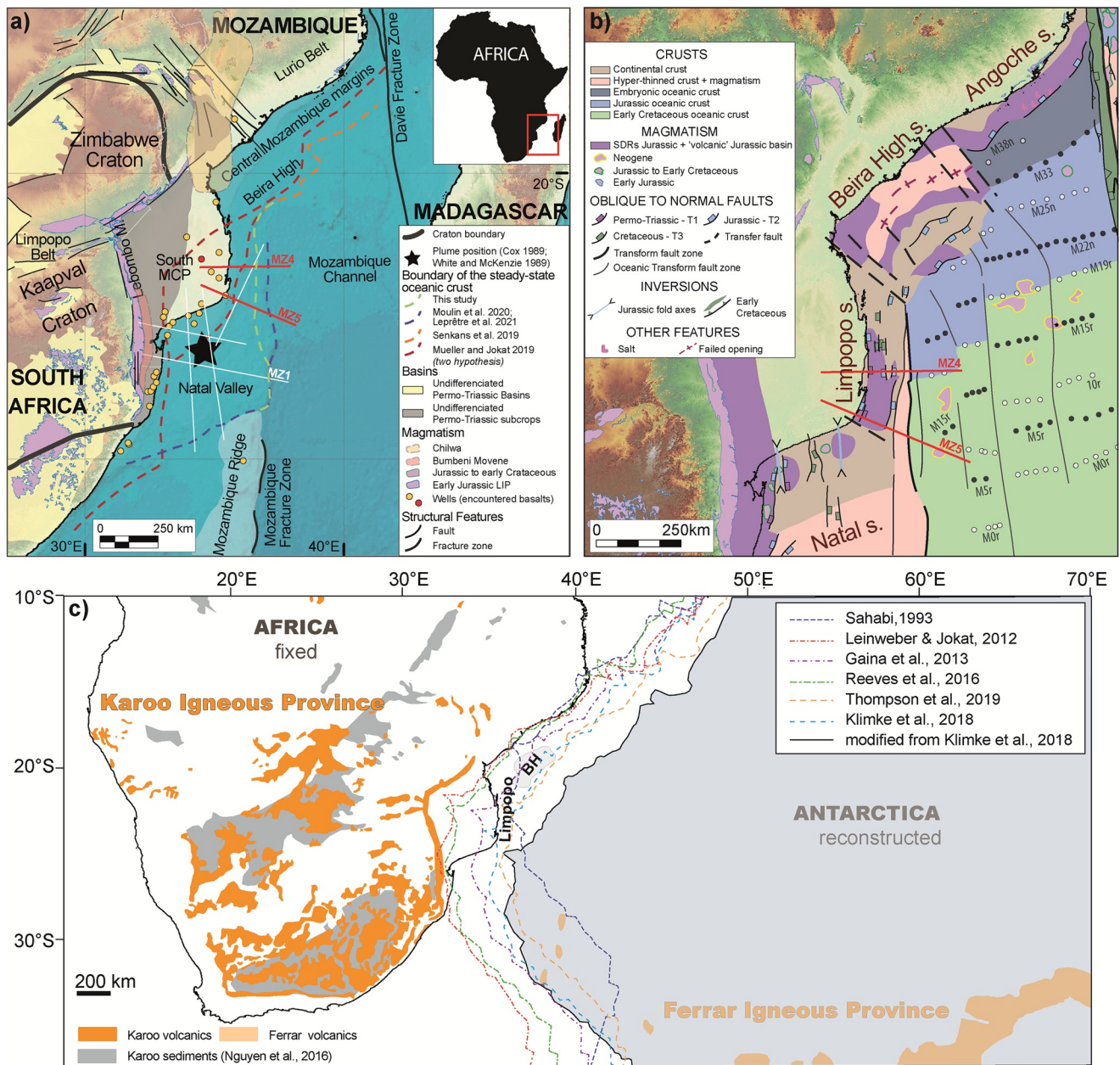


Figure 1. Location map of the study area and geodynamic context of the Limpopo transform margin and Mozambique Channel. (a) Map of the Mozambique margin and Channel. LIP: Large Igneous Province, MCP: Mozambique Coastal Plain, AAC: Africa-Antarctica Corridor. The well shown in red contains basalts dated in Roche et al. (in rev., this journal) at 181–186 Ma (Karoo). (b) Structural context of the study area (Roche et al., in rev.; modified from Castilla et al., 2015; Senkans et al., 2019). White and black dots are magnetic anomaly identifications and thin black lines are the denote oceanic transform fault zones (after Leinweber & Jokat, 2012; Mueller & Jokat, 2017, 2019). (c) Map of the areal extent of the Karoo Igneous Province and the associated Karoo sediments (Nguyen et al., 2016) in the African continent. The Ferrar Igneous Province is located in the Antarctica continent, which is shown in its reconstructed position before the opening of the Mozambique basin (modified from Klimke et al., 2018). Dashed lines show the reconstructed positions proposed by the various kinematic models listed in the legend (Gaina et al., 2013; Klimke et al., 2018; Leinweber & Jokat, 2012; Reeves et al., 2016; Sahabi, 1993; Thompson et al., 2019).

Magmatic activity played an important role throughout the geological history of the region. The Karoo and Ferrar Large Igneous Provinces (LIP), in Africa and Antarctica, respectively (Jourdan et al., 2009), are associated with the rifting and dispersal of Gondwana, during the Early Jurassic. Most of the Karoo LIP volcanism occurred between 184 and 177 Ma (Jourdan et al., 2007). This thick series of basalts (White & McKenzie, 1989), mainly crops out in the Lebombo Monocline, just west of the Mozambique Coastal Plain (Klausen, 2009, Figure 1a). The origin of this magmatic province is still controversial and may be associated with a mantle plume activity

or with decompression melting due to divergent far-field forces (e.g., Cox, 1989; White & McKenzie, 1989; Jourdan et al., 2007; Klausen, 2009; Hastie et al., 2014; Peace et al., 2019). Subsequently, magmatic activity became more widespread, occurring throughout the Mozambique Channel (e.g., the Mozambique Ridge, Figure 1). This widespread magmatic activity ranges in age from the Lower Cretaceous (Erlank & Reid, 1974; Fischer et al., 2017; König & Jokat, 2010; Thompson et al., 1982) in the south Natal Valley to Mid-Miocene-to-present in the Natal Valley and the areas south of Beira High and Angoche segments (Ben-Avraham et al., 1995; Courgeon et al., 2017, 2018; Deville et al., 2018). This volcanic activity may have been associated with a large, deep, and long-lived thermo-chemical anomaly that may be the source of the Karoo LIP volcanism as well as the present day Afar mantle plume (e.g., Jacques et al., 2019; O'Connor et al., 2019; Torsvik & Cocks, 2013; Torsvik et al., 2006).

The entire Mozambique margin shows clear indications of a rifting stage during the emplacement of the Karoo LIP, before the transform motion (e.g., Roche et al., 2021; Senkans et al., 2019; Vormann et al., 2020). This rifting stage is characterized by intense syn-rift magmatic activity that is observed both offshore and onshore as evidenced by the seaward dipping reflectors at Angoche margin and magmatic sills and volcano-clastic material at Beira High (Senkans et al., 2019), as well as basalts, including some below Cretaceous sediments, found in wells (Flores, 1984; Ponte et al., 2019; Raillard, 1990; Salman & Abdula, 1995). The onshore outcropping Proterozoic basement consists of a Precambrian orogenic zone, the Mozambique Belt, along the northern part of Beira High and Angoche segments, and the Kaapval craton along the Lebombo Monocline (Figures 1a and 1b; Daly et al., 1989). Northwest-southeast trending extension resulted in continental break-up followed by seafloor spreading, which occurred in the Angoche segment first (Figure 2). Recent seismic reflection profiles crossing the Central Mozambique margins (Angoche and Beira High segments) show that the peculiar oceanic crust seismic facies is not apparent before chron 33n (161 Ma) in the Angoche segment and chron 25n (156 Ma) in the Beira High segment (Figure 1b; Senkans et al., 2019). The onset of seafloor spreading in the Beira High segment may have been slightly delayed by the formation and failure of the northern Beira High rift (Figure 1b; Senkans et al., 2019) and polyphase seafloor spreading as proposed by Mueller and Jokat (2019).

The deformation style along the Limpopo margin varies from oblique rifting resulting from NW-SE extension during the Kimmeridgian (stage TF1, Figure 2), to transform motion resulting from N-S extension during the Barremian (stage TF4, Figure 2). During the intermediate stages (TF2 and TF3, Figure 2), the orientation of extension rotated, leading to the formation of a trans-tensional faulting system along the margin, with a wide zone affected by shear deformation. The two profiles presented in this study cross the transform fault system and, together with industry seismic reflection data, the velocity models provide clear insight into the nature and geometry of the crust, as well as the occurrence of magmatic activity.

3. Data Acquisition and Processing

The seismic refraction and collocated multi-channel seismic data used in the study were acquired during the MOZ 3/5 cruise in 2016 (Moulin & Aslanian, 2016; Moulin & Evain, 2016). We used additional high-resolution multi-channel seismic reflection profiles for the seismic interpretation acquired by INP - WesternGeco in 2013. The seismic refraction data (Watremez et al., 2021) allowed us to build velocity models at crustal scale, while the coincident commercial and academic seismic reflection profiles allowed us to image and model shallow structures, particularly the uppermost basement.

3.1. MOZ 3/5 Survey

In this study, we present the results of the P-wave velocity modeling along two seismic refraction profiles crossing the East Limpopo Margin: MZ4 and MZ5 (Figures 1 and 3). The two profiles were acquired across the transform margin, but with slightly different orientations.

The two profiles were acquired using a 6,500 in³ source (i.e., 107 L, using 15 airguns), fired every 60 s (~155-m spacing), and synchronized on the first peak (Avedik et al., 1993). A total of 1,504 and 1,882 shots were recorded by all instruments along MZ4 and MZ5, respectively. Data were recorded by 16 ocean bottom seismometers (OBS) and 18 on land seismometers along MZ4, and 22 OBSs and 16 on land seismometers along MZ5. The lengths of the profiles, from the westernmost on land seismometer to the easternmost shot, are ~360 and

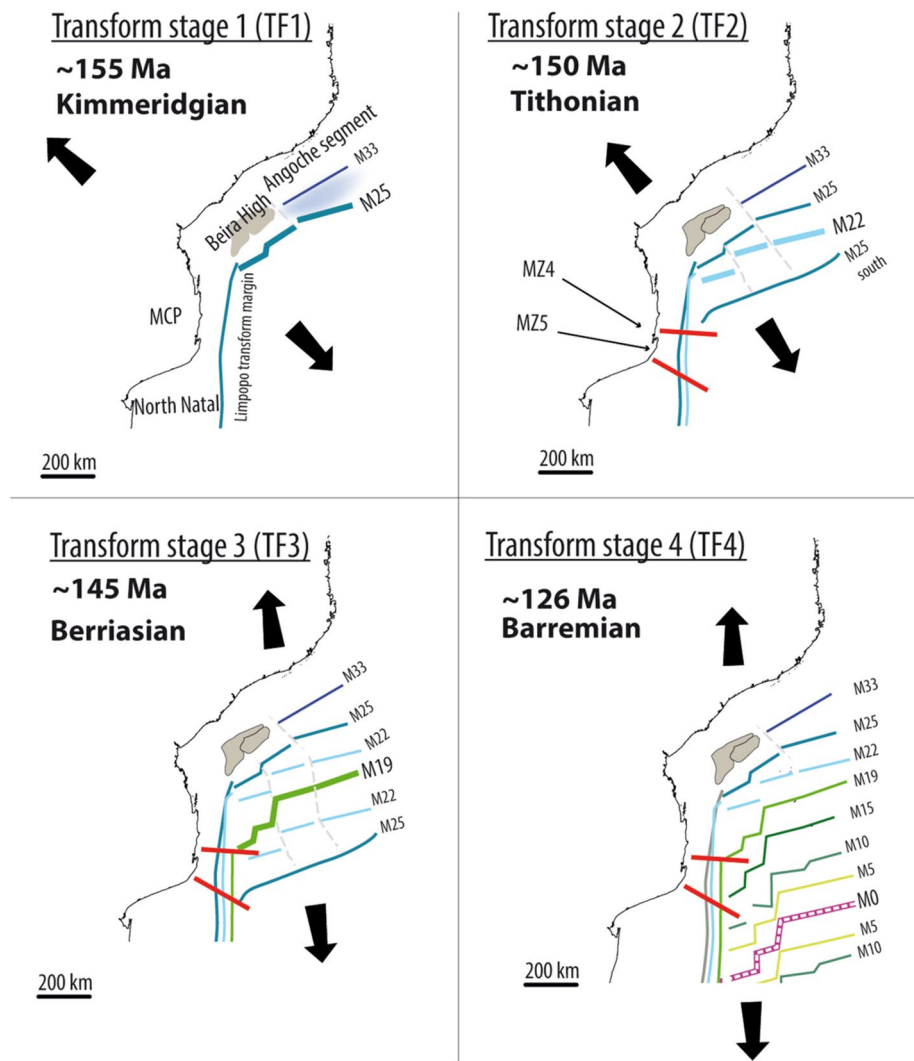


Figure 2. Series of sketches showing the evolution of the central Mozambique area and the Limpopo magma-rich transform zone based on a study of the Angoche and Beira High segments by Senkans et al. (2019), our study and that of Roche et al. (2021). Isochrons modified from Mueller and Jokat (2019). Red lines show the location of the seismic profiles. Transform stage 1 (TF1): Initiation of the transform fault zone may have occurred at 155 Ma as seafloor spreading, oriented NW-SE, began along the Beira High and Antarctica conjugate margins. Transform stage 2 (TF2): The opening of the oceanic basin continues with the spreading center migrating southward. Transform fault stage 3 (TF3). The direction of opening and the transform fault have become slightly oblique to the Limpopo transform margin. Transform fault stage 4 (TF4): the direction of extension trended NS during T4.

~400 km for MZ4 and MZ5, respectively. Data were picked at source-receiver distances of up to 330 km using Zplot, an interactive picking and visualization software for seismic data, developed by C. Zelt.

Instrument spacing was 12 and ~3 km offshore and onshore, respectively. All the OBSs were 4-components-instruments (hydrophone and three-component-geophone; vertical, transverse, and radial) and were relocated on-board using the arrival times from the closest shots. On land seismometers along the profiles were all three-component-geophones. The data acquired along the two profiles generally have high signal-to-noise ratios, for both OBSs and on land seismometers. However, the signal tends to be noisier on instruments that are close to the coast-line due to factors such as dense marine traffic and waves. Frequencies of data collected by the OBS hydrophones are usually higher than that collected by OBS vertical geophones at short source-receiver distances (hereafter “offsets”), while OBS vertical geophones record high amplitude signals at larger offsets than hydrophones. Thus, we used both data sets for our processing.

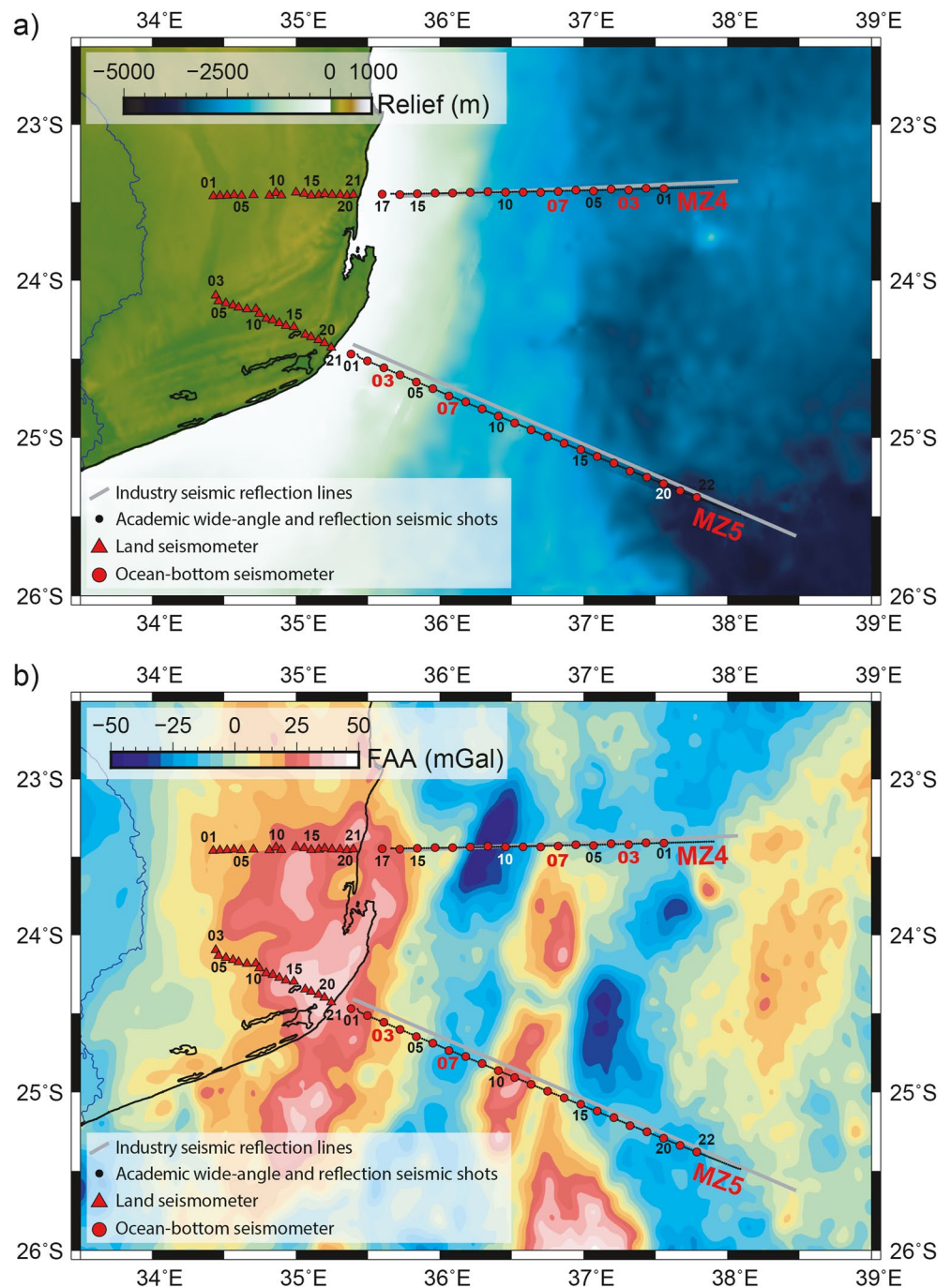


Figure 3. Location of the profiles used in this study and (a) bathymetry map, and (b) free-air gravity anomaly map. The bathymetry data from the GMRT compiled data set (Ryan et al., 2009) and the MOZ 3/5 cruise data. The free-air gravity anomaly data from the Sandwell and Smith (2009) data (v18.1).

Collocated seismic reflection data were acquired as the refraction shots were recorded, on a 4,500-m-long solid streamer section with 720 channels distributed every 6.25 m. On-board processing was carried out using the Geo-cluster software (CGG-Veritas). The main processing sequence consisted of external mute of the direct wave and water column, wideband filter (1–8–64–92 Hz), predictive deconvolution, surface-related multiple elimination, normal move-out correction, time-dependent bandpass filtering, external mute of the seabed, and associated refractions, and stacking. Finally, a Kirchhoff migration was applied before stacking the pre-processed data.

Collocated potential field data were also acquired during the MOZ 3/5 cruise. Free-air gravity anomaly data were acquired using a KSS31M gravimeter located near the ship's center of gravity, and magnetism data were acquired using an SMMII magnetometer attached at the end of the seismic streamer to prevent the ship's magnetic field from influencing the signal.

3.2. Method, Phase Picking, and Uncertainties

Two primary methods are generally used to process travel time arrivals from wide-angle seismic data to generate a velocity model: forward modeling and travel-time tomography. In this study, we used the Rayinvr forward modeling scheme developed by Zelt and Smith (1992). Model parameters consist of interface depth nodes, the depth of the interface being linearly interpolated between two nodes, and velocity nodes located at the interfaces (just above and/or just below, allowing for velocity contrasts at each interface). The aim of forward modeling is to build a velocity model with the smallest number of parameters as possible that correlates well with the data, lying within the data uncertainty range ("minimum parameter" or "minimum structure" approach in Zelt, 1999). We followed a layer stripping strategy, working first with the arrivals at short offsets (uppermost layers), and building the model from top to bottom, including arrivals at larger offsets, that is, that traveled in deeper (higher P-wave velocities) structures (Zelt, 1999). Rayinvr also has an inversion scheme, but it is not efficient when the model structure is complicated by layers pinching out, velocity inversions with depth, and/or strong lateral velocity variations. However, this inversion feature can be useful for resolution assessment (see Section 3.3 Resolution assessment and Zelt, 1999). We also ran Tomo2D (Korenaga et al., 2000) layer-stripping inversions using the same method as Sallarès et al. (2011) for the offshore parts of both models, giving similar but smoother results than those obtained with Rayinvr (see Section S1 in Supporting Information S1 for more details).

The first step of forward modeling is to identify the different seismic phases on each seismic record, starting from the arrivals at short offsets (i.e., arrivals from the uppermost layers). Table 1 links the phase codes and interpretation of the typical velocities. This interpretation can vary slightly near the sediment/crust interface and will be discussed later in the text; Table 1 must be considered as a guide.

Most of the seismic phases can be identified by comparing the signal and apparent velocities from one instrument to another, while maintaining lateral velocity continuity to respect the minimum parameter approach during modeling. For the shallowest layers, that is, the sediments, we compared the arrival times of reflected arrivals at normal incidence along the OBS records with the seismic reflection profile to help define which phases to use in the sediments.

Building a minimum structure model involves modeling the smallest number of layers possible. Thus, an interface in the velocity model may differ from a geological interface observed on the seismic reflection data, especially in sediments. An example of phase identification in the sediments is shown in Figures 3a and 3b. The hyperbola shaped arrivals in the central part of the record correspond to the intra-sedimentary reflections that were picked following the comparison with the seismic reflection profile, in two-way travel time. We chose the sediment reflections that could be associated with refracted arrivals in the layer above the reflection and that had an apparent velocity close to the reflections at larger offsets. Some other arrivals could be seen with apparent velocities typical for sediment phases but are interpreted as converted S-wave arrivals. Indeed, they show comparable features to P-waves, but with slower apparent velocities. For example, the clear set of arrivals dipping down from 2 to 4 s at offsets >10 km (in Figure 4a) corresponds to a seismic phase that propagated as refracted S-waves in the crust.

Deeper phases are defined using the apparent velocities of the refracted phases while always trying to limit lateral velocity variations within a layer (minimum structure). Examples of phase identification in the crust and uppermost mantle are shown in Figures 4b–4d (down to upper-crust and, to lower-crust and to uppermost mantle, respectively). This phase identification process allowed us to identify a total of 68,719 and 75,920 arrival times on the OBS and land-seismometers record sections of MZ4 and MZ5, respectively.

To assess the fit between the data (i.e., picks) and the model (i.e., computed arrival times), uncertainty values must be assigned to the picked arrival times. These uncertainties are set by an automatic process as a function of the signal-to-noise ratio, independent of the user and the picked phase (Zelt, 1999). Zelt and Forsyth (1994) used an empirical relationship to define the uncertainties using the signal-to-noise ratio of the seismic trace of 250 ms before and after the pick. However, this relationship was defined in 1994, and the data available today have a greater number of shots within a given distance, and source signals have been improved (wider range of

Table 1
Description of the Model Phases

Phase	Description
1.0	WW – Direct arrival in the water
2.1	Sed1 – Refraction in the first sediment layer
2.2	Sed1R – Reflection at the base of the first sediment layer
3.1	Sed2 – Refraction in the second sediment layer
3.2	Sed2R – Reflection at the base of the second sediment layer
4.1	Sed3 – Refraction in the third sediment layer
4.2	Sed3R – Reflection at the base of the third sediment layer
5.1	Sed4 – Refraction in the fourth sediment layer
5.2	Sed4R – Reflection at the base of the fourth sediment layer
6.1	Sed5 – Refraction in the fifth sediment layer
6.2	Sed5R – Reflection at the base of the fifth sediment layer
7.1	Sed6 – Refraction in the sixth sediment layer
7.2	Sed6R – Reflection at the base of the sixth sediment layer
8.1	Sed7 – Refraction in the seventh sediment layer
8.2	Sed7R – Reflection at the base of the seventh sediment layer
9.1	Sed8 – Refraction in the eighth sediment layer or the uppermost basement
9.2	Sed8R – Reflection at the base of the eighth sediment layer or uppermost basement
10.1	Pg1 – Refraction in the upper-crust
10.2	PgP – Reflection at the intra-crustal boundary
11.1	Pg2 – Refraction in the lower-crust
11.2	PmP – Reflection at the Moho discontinuity
12.1	Pn – Refraction in the uppermost mantle

Note. The left column presents the phase names used during modeling: the first number is the deepest layer in which the ray is traced and the second number describes the type of propagation (0 for direct waves, 1 for refractions, and 2 for reflections at the base of the considered layer).

frequencies), probably leading to overestimates of this uncertainty, especially at short offsets. Therefore, we decided to use a slightly modified version of Zelt and Forsyth's (1994): we reduced the uncertainties for offsets <30 km (see Section S2 in Supporting Information S1). This way, an objective value of picking uncertainty in time, was automatically assigned to each pick.

3.3. Resolution Assessment

The modeling statistics consist of the number of rays traced in the model (N), the root-mean-squared travel time residual (t_{RMS}), and the normalized chi-square (χ^2). χ^2 corresponds to the average misfit between the theoretical and picked travel times, with respect to the picking uncertainty. A χ^2 reduced to ~ 1 means that the phase/model correlates well with the picks, falling within their uncertainty margins (Bevington, 1969). Table 2 presents the modeling statistics for each phase and each model. Thus, the two models correlate well with the data, when χ^2 values are close to 1. Almost 94% of these picks are actually modeled after the ray-tracing in each model. Section S3 in Supporting Information S1 presents all the fits for each instrument used in this study. Despite similar values of χ^2 , the t_{RMS} values tend to be greater along MZ4 than along MZ5. This is due to the fact that the signal-to-noise ratio is generally higher along MZ5 than along MZ4.

Another test that can be used is to assess the sensitivity of the model to perturbations of the model parameters (i.e., velocities or interface depths) by plotting t_{RMS} values for different sets of perturbations (e.g., Leprêtre et al., 2013). We present the results of this test as velocity anomaly diagrams (see Section S4 in Supporting Information S1). This test is useful in that it provides an estimate of the range of uncertainty for the velocities within the crust/uppermost mantle and for the depth of the Moho. For example, a 0.1 km/s velocity perturbation in the lower crust

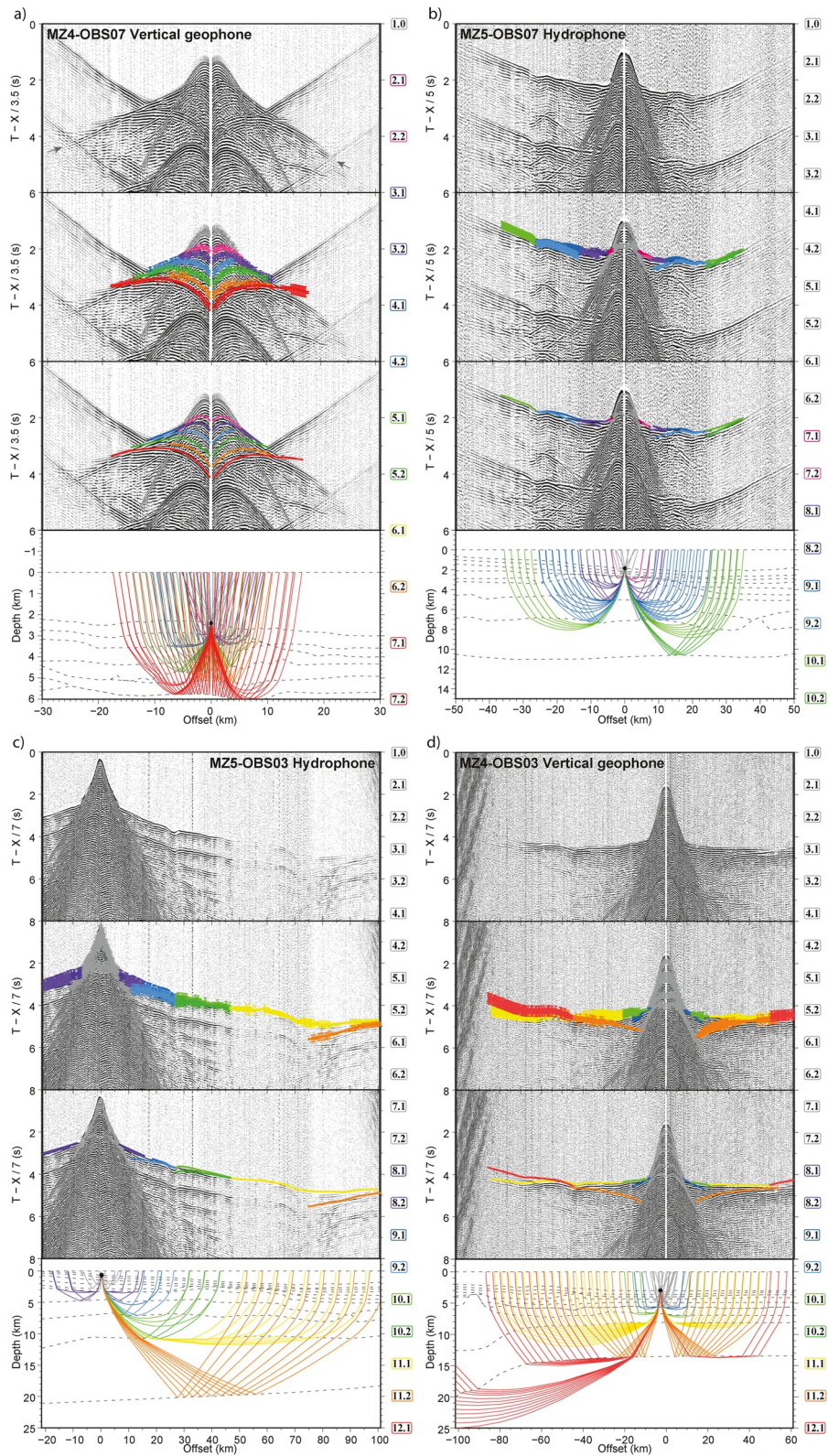


Figure 4.

Table 2
Modeling Statistics

Phase	MZ4			MZ5		
	<i>N</i>	t_{RMS}	χ^2	<i>N</i>	t_{RMS}	χ^2
1.0	956	24	0.419	1,414	17	0.142
2.1	174	27	0.679	113	33	0.358
2.2	725	22	0.294	1,063	26	0.445
3.1	343	25	0.577	471	29	0.482
3.2	1,042	22	0.291	1,659	27	0.499
4.1	445	22	0.467	595	27	0.322
4.2	916	25	0.562	2,331	28	0.499
5.1	102	25	0.699	86	31	0.48
5.2	832	38	0.854	1,021	28	0.387
6.1	65	22	0.704	85	30	0.562
6.2	946	41	1.826	1,140	31	0.611
7.1	418	25	0.706	190	31	0.487
7.2	2,071	33	1.146	697	30	0.771
8.1	147	37	0.879	1,349	33	0.306
8.2	59	47	0.618	759	32	0.147
9.1	1,949	32	0.978	1,806	31	0.582
9.2	387	44	0.825	2,024	33	0.584
10.1	3,880	52	1.152	5,528	46	0.615
10.2	1,845	77	1.075	3,070	63	0.712
11.1	16,490	96	1.035	19,860	66	1.123
11.2	12,599	120	1.214	12,948	88	1.609
12.1	17,840	134	1.151	13,074	90	1.892
Total	64,231	103	1.073	71,283	68	1.138

Note. *N*: number of rays traced in the model; t_{RMS} : root-mean-squared travel time residual (ms); χ^2 : normalized chi-square.

or the uppermost mantle leads to a significant increase of the residual travel times (>50 ms) for both profiles (Section S4 in Supporting Information S1).

The velocity models are presented together with their quantitative resolution results (Figures 5 and 6). We present the values of the diagonal of the resolution matrix (Figures 5 and 6b) and the acceptable velocity deviations from the velocity model using a Monte Carlo analysis (Figures 5c, 5d, 6c and 6d).

The resolution of each velocity and interface depth nodes can be assessed using the value of the diagonal of the resolution matrix obtained from the inversion scheme of Rayinvr (Zelt, 1999). A value of the diagonal of the resolution matrix below 0.5 is considered fair, values above 0.5 are considered good, and values above 0.75 are considered very good. Both diagrams of the value of the diagonal of the resolution matrix show good to very good resolution throughout the velocity models (Figures 5 and 6b). In particular, (a) resolution is close to one in the crustal layers; (b) it is still good but with more variability in the sedimentary layers, depending on the number of picks modeled and potential presence of low velocity zones, thin layers, and pinch-outs; and (c) it is also lower at the ends of the sections, at model distances lower than the landward-most shot and greater than the seaward-most OBS; that is, in areas where seismic rays traveled in only one direction. Similarly, the resolution of the interface depth nodes in the crust is also very good, except where layers pinch-out (MZ5, model distances of 110–120 km and 140–150 km, 6–7 km depth, Figure 6). However, such high-resolution values in the crust are meaningless. Therefore, we ran a quantitative resolution analysis in the crustal layers using VMonteCarlo.

VMonteCarlo (Loureiro et al., 2016) is an automatic procedure that tests the values for the velocity and interface depth nodes within a certain range and quantitatively assess their resolution. Here, we use this procedure for the crustal and uppermost mantle layers. The velocity and depth nodes in the crust and uppermost mantle were randomly perturbed following the parametrization scheme in Table 3. The choice of the introduced perturbations was guided by the results of the velocity anomaly diagrams (see Sections S4 and S5 in Supporting Information S1) and test runs with VMonteCarlo. VMonteCarlo was set for 50,000 runs along each profile. Rays were successfully traced in a total of 39,661 and 38,362 models along MZ4 and MZ5, respectively. Threshold criteria chosen for the computation of the uncertainty

maps were selected as follows: (a) the perturbed model would allow for at least 90% of the rays of the original model to be traced, (b) t_{RMS} should be less than 1.5 times the t_{RMS} of the final model, and (c) the χ^2 should be less than twice the final model χ^2 . The models that did not meet these thresholds were discarded. A total of 5,975 and 1,040 models met these criteria along MZ4 and MZ5, respectively. This difference in number of models is due to the fact that the signal-to-noise ratio is higher for MZ5 data. Therefore, average uncertainties along MZ5 are lower than along MZ4. Thus, the limit χ^2 is met for smaller model variations along MZ5 than MZ4. The results of the VMonteCarlo analysis show that the crustal and uppermost mantle velocities are usually well resolved along both lines, with uncertainties <300 m/s (Figures 5c, 5d, 6c and 6d). Larger uncertainty values occur near the interfaces because of the uncertainty of the interface depth nodes. The uncertainty of the interface depth nodes is approximately ± 500 m along both lines for both mid-crust and Moho interfaces. Highest velocity standard deviations are observed at the Moho interface along both models. This is due to the fact that some valid models may place the

Figure 4. Examples of data (top panels in a, b, c, and d), picked arrivals with colored uncertainty bars (second panels from the top), computed arrivals (third panels from the top), and raytracing (bottom panels) in different parts of the model. A bandpass filter (1–5–18–25 Hz) was applied for display only. MZ4-OBS07 (a) shows data and interpretations in the sediment layers, MZ5-OBS07 (b) shows data and interpretations down to the transform domain, MZ5-OBS03 (c) shows data and interpretations down to the lower crust in the continental domain, and MZ4-OBS03 (d) shows data and interpretations in the crustal and mantle layers, in the oceanic domain. The color code for the rays and picks is shown on the right of the plots and refers to model phases detailed in Table 1. The gray arrows in the top panels show S-wave arrivals (not used in this study).

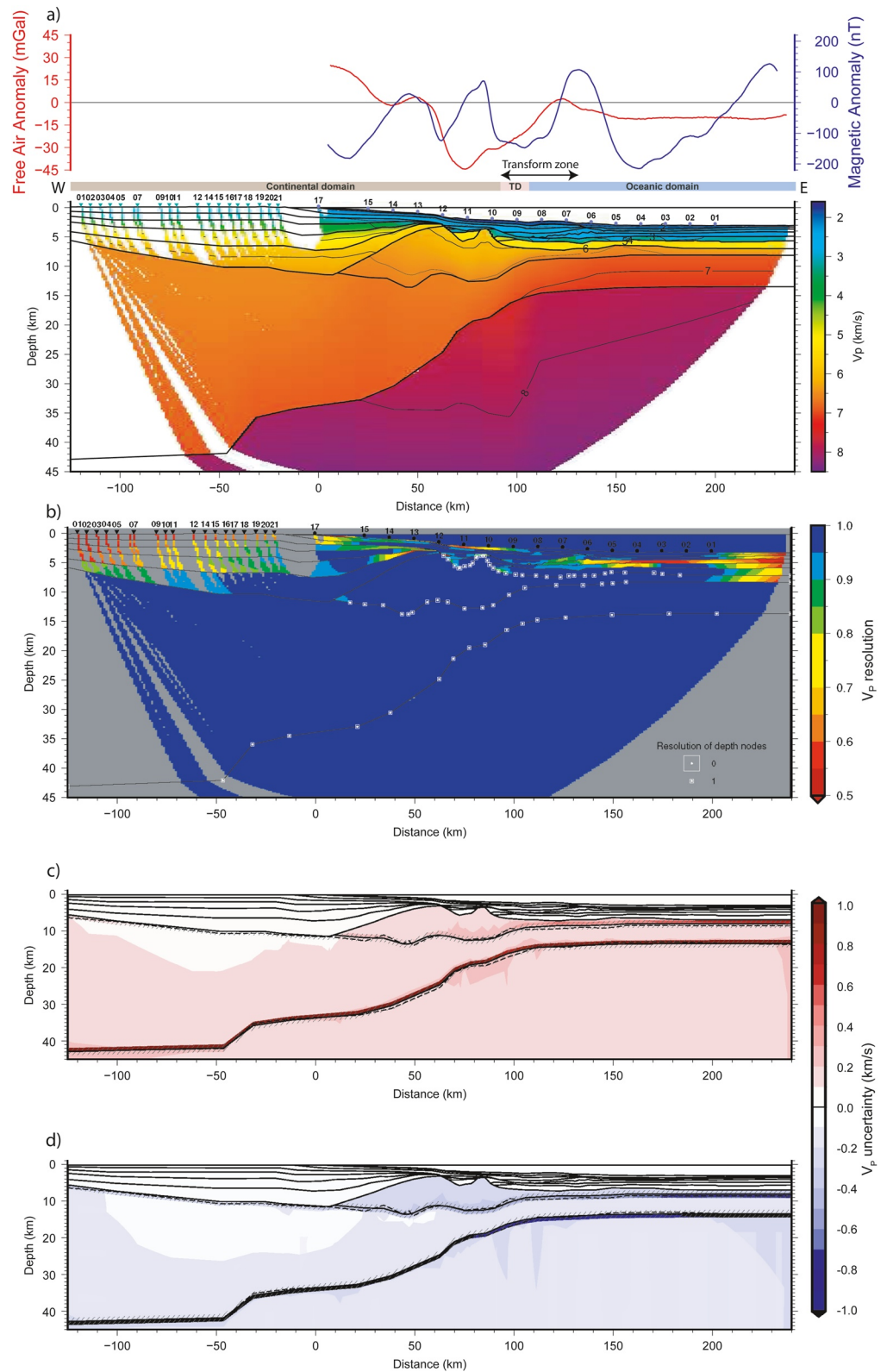


Figure 5. Velocity modeling results along MZ4. (a) P-wave velocity model. The free-air gravity and magnetic anomalies acquired during the cruise are shown above the model. (b) Diagonal of the resolution matrix. (c)–(d) Maximum and minimum admissible velocity deviations from the preferred model shown in (a) obtained using VMonteCarlo, with maximum perturbations set in Table 3. Color scales are shown next to each plot.

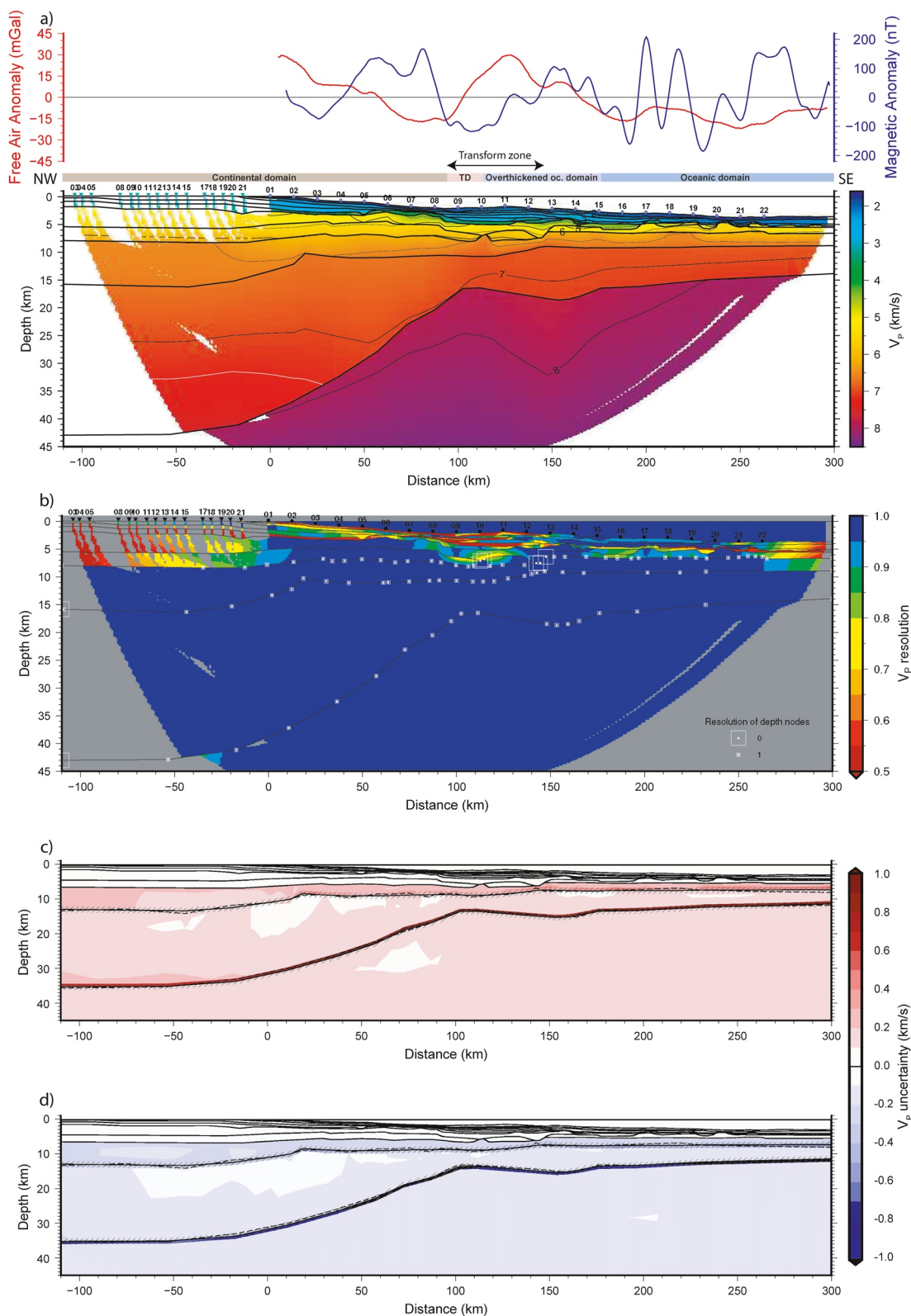


Figure 6. Velocity modeling results along MZ5. (a) P-wave velocity model. The white line shows the 7.2 km/s iso-velocity contour. The free-air gravity and magnetic anomalies acquired during the cruise are shown above the model. (b) Diagonal of the resolution matrix. (c)–(d) Maximum and minimum admissible velocity deviations from the preferred model shown in (a) obtained using VMonteCarlo, with maximum perturbations set in Table 3. Color scales are shown next to each plot.

Table 3
Maximum Allowed Parameter Perturbations for Each Set of Parameters for VMonteCarlo

Set of parameters	Parameters MZ4	Parameters MZ5	Max. Perturbation
V_p top of upper-crust	1–16	1–23	± 0.25 km/s
V_p base of upper-crust	17–28	24–38	± 0.25 km/s
Depth of intra-crustal interface	29–56	39–65	± 1 km
V_p top of lower-crust	57–64	66–72	± 0.1 km/s
V_p base of lower-crust	65–71	73–78	± 0.2 km/s
Depth of Moho	72–89	79–97	± 1 km
V_p top of mantle	90–95	98–104	± 0.2 km/s
V_p top of mantle	96–97	105–106	± 0.2 km/s

Note. The parameter numbers for each model correspond to a sequential number of perturbed parameters (see Section S4 in Supporting Information S1 for the location of each parameter along both lines).

Moho above this area, and others below. Thus, the standard deviation in this ~ 1 km layer around the Moho is approximately equal to the velocity contrast at the Moho. Conversely, the upper part of the lower crust in the continental domain (model distances < 50 km) shows the lowest velocity standard deviations, indicating very good resolution in this area. However, only a few nodes (model distances < 0 km) define the velocity fields in the westernmost part of the models and the velocity gradient is low in this area. Thus, the χ^2 and t_{RMS} values are strongly sensitive to the velocity perturbations, leading to a low uncertainty in this area. The VMonteCarlo standard deviations are generally greater than that suggested by the velocity anomaly diagrams (see Section S4 in Supporting Information S1).

4. Results and Interpretation

Transform margins typically show a narrow transition domain between continental and oceanic domains. P-wave velocity models, arrived at by interpretation of the seismic refraction data, are used to distinguish the different crustal domains and the thickness of the crust. Wide-angle reflections are used to model discontinuities, in particular the Moho as the interface separating typical crustal velocities (< 7.5 km/s) from typical mantle velocities

(> 7.8 km/s). The continental crust generally exhibits up to three layers, with velocities of 5.7 to 7–7.2 km/s, increasing with depth (Christensen & Mooney, 1995) and a total thickness of up to 40 km. In contrast, oceanic crust usually shows the typical Penrose oceanic layering with a high velocity gradient layer 2 (L2a/L2b) and a low velocity gradient layer 3 (L3), with a total thickness of ~ 6 –8 km (Christeson et al., 2019; White et al., 1992). In the transitional domain, it can be difficult to distinguish thinned continental crust from oceanic crust. Seismic reflection data from nearby our profiles (see location in Figure 2), provide further constraints on the shallowest structures.

The P-wave velocity models along the two crustal transects MZ4 and MZ5 are shown in Figures 5a and 6a. Figures 7 and 8 present subsets of high-quality industry seismic reflection profiles (top panels), to be compared with the P-waves velocity models overlain by the collocated MOZ 3/5 seismic reflection data (bottom panels). The results show clearly delineated continental, transitional, and oceanic domains along both profiles, as well as indications of magmatic activity and transform motion at fault zone (Figures 2, 5 and 6). The westernmost parts correspond to the continental domain characterized by crustal necking up to model distances of 90 km along MZ4 and 95 km along MZ5. The easternmost parts correspond to the oceanic domain, defined as a zone showing little lateral velocity variations and measuring model distances greater than 150 and 170 km along MZ4 and MZ5, respectively. Between the continental and oceanic domains is a transitional domain. We discuss the nature of these domains in detail below.

4.1. The Continental Domain

Average P-wave velocity models in the continental domain consist of the water column, seven sediment layers, one or two crustal layers, and a mantle layer (Figures 5 and 6). Seismic refraction velocities provide further constraint on the position of the sediment-crust boundary, which is sometimes below the acoustic basement (e.g., Figure 8a at model distances of 20–50 km). The P-wave velocity model of MZ4 highlights a landward thickening wedge (Figure 5a, model distances 0–60 km). This wedge corresponds to a series of landward dipping reflections in the collocated multi-channel seismic data (Figure 7a), and shows velocities up to 6.2 km/s indicating thicknesses up to 12 km. Some bright reflectors suggest magmatic material filling this wedge (Figure 7a). This feature is interpreted as a volcano-sedimentary sequence. A similar structure exists along MZ5 (Figure 8a), where the velocity model shows slightly lower velocities (< 6.5 km/s) in the crust (model distances > -30 km, Figure 5). The same reflectivity pattern is observed along both lines (compare the “Landward dipping reflectors” in Figures 7a and 8a). Thus, seismic reflection data show that this wedge is present in both profiles, whereas it does not appear in the velocity model layering along MZ5 (Figure 8a). Indeed, the seismic velocities beneath the acoustic basement in this part of MZ5 show values of ~ 5 km/s, similar to those for the upper part of the prism along MZ4. The detailed structure and formation of this volcano-sedimentary prism are discussed by Roche et al. (2021). The

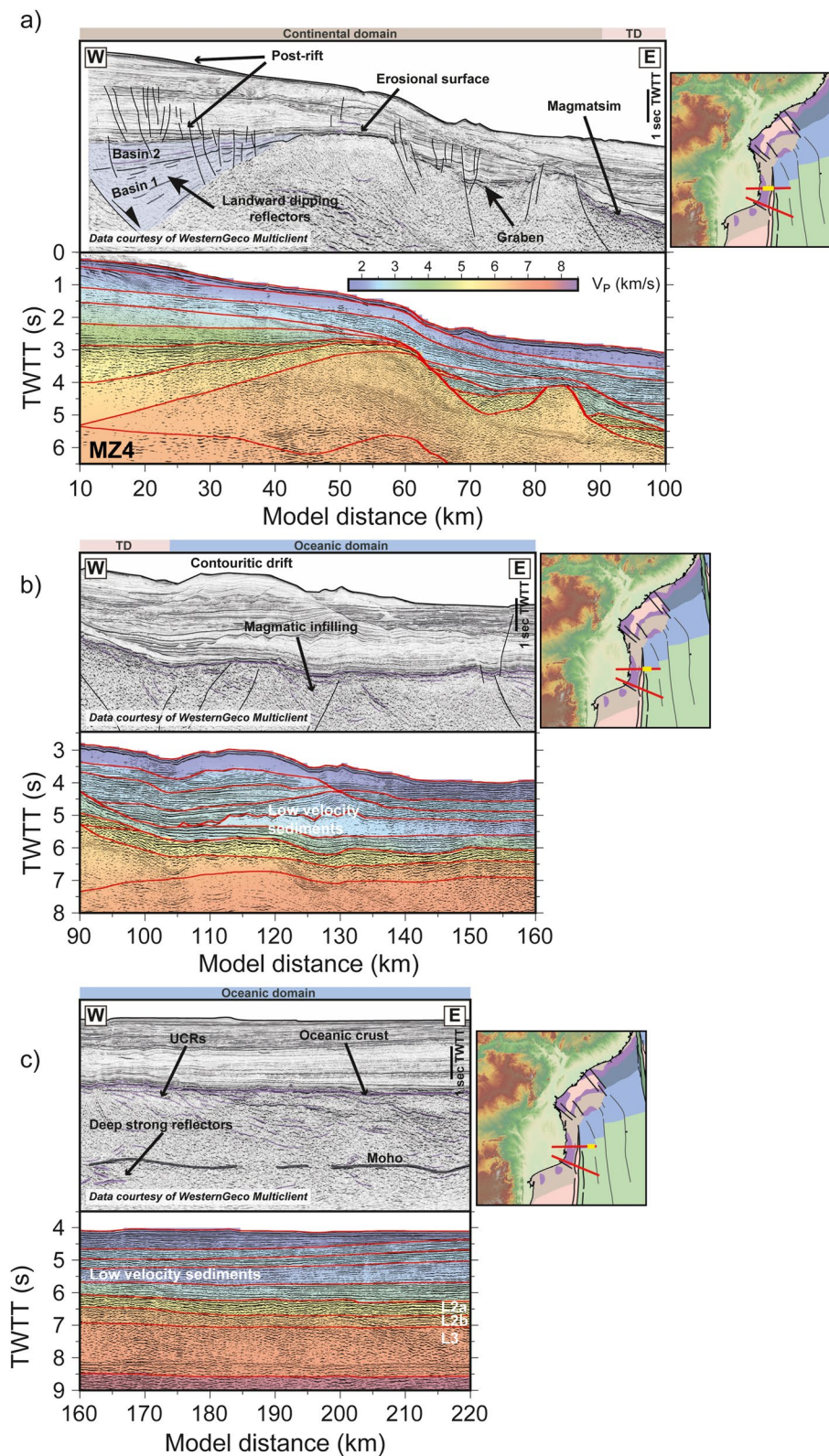


Figure 7. Comparison of subsets of MZ4 velocity model with collocated seismic reflection data. (a) Subsets of the sections in the continental domain. (b) Subsets of the sections showing the transitional domain. (c) Subsets of the sections in the oceanic domain. Top panels: Un-interpreted depth migrated coincident INP and WesternGeco Multiclient profile. Bottom panels: Superposition of the collocated time-migrated seismic reflection profile acquired during the MOZ 3/5 cruise, with the time-converted model interfaces (red lines) and velocity model, to permit comparison of the velocity models with the reflectivity.

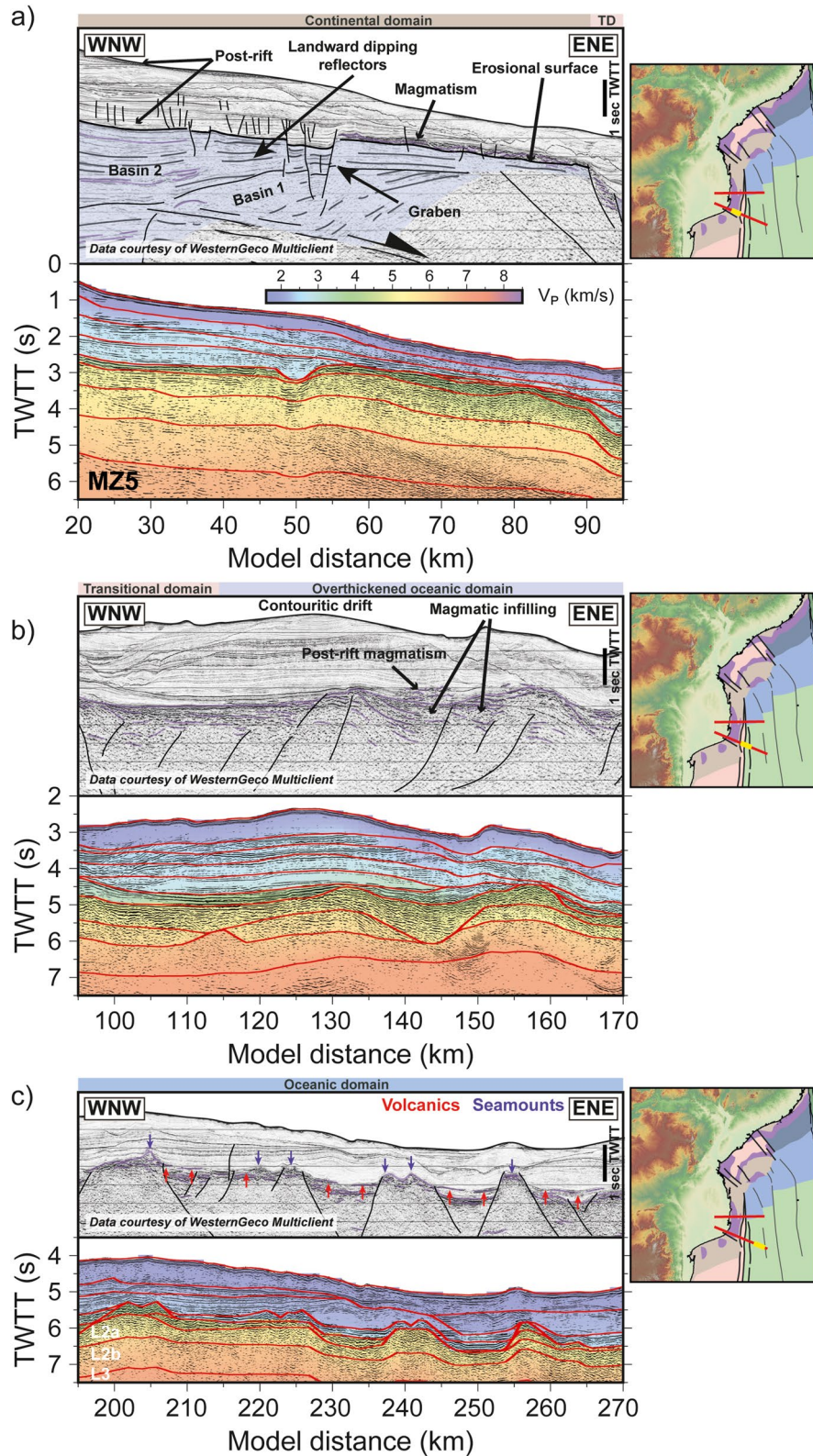


Figure 8. Comparison of subsets of MZ5 velocity model with collocated seismic reflection data. (a) Subsets of the sections in the continental domain. (b) Subsets of the sections showing the transitional domain. (c) Subsets of the sections in the oceanic domain. Top panels: Un-interpreted depth migrated coincident INP and WesternGeco Multiclient profile. Bottom panels: Superposition of the collocated time-migrated seismic reflection profile acquired during the MOZ3/5 cruise, with the time-converted model interfaces (red lines) and velocity model, to permit comparison of the velocity models with the reflectivity.

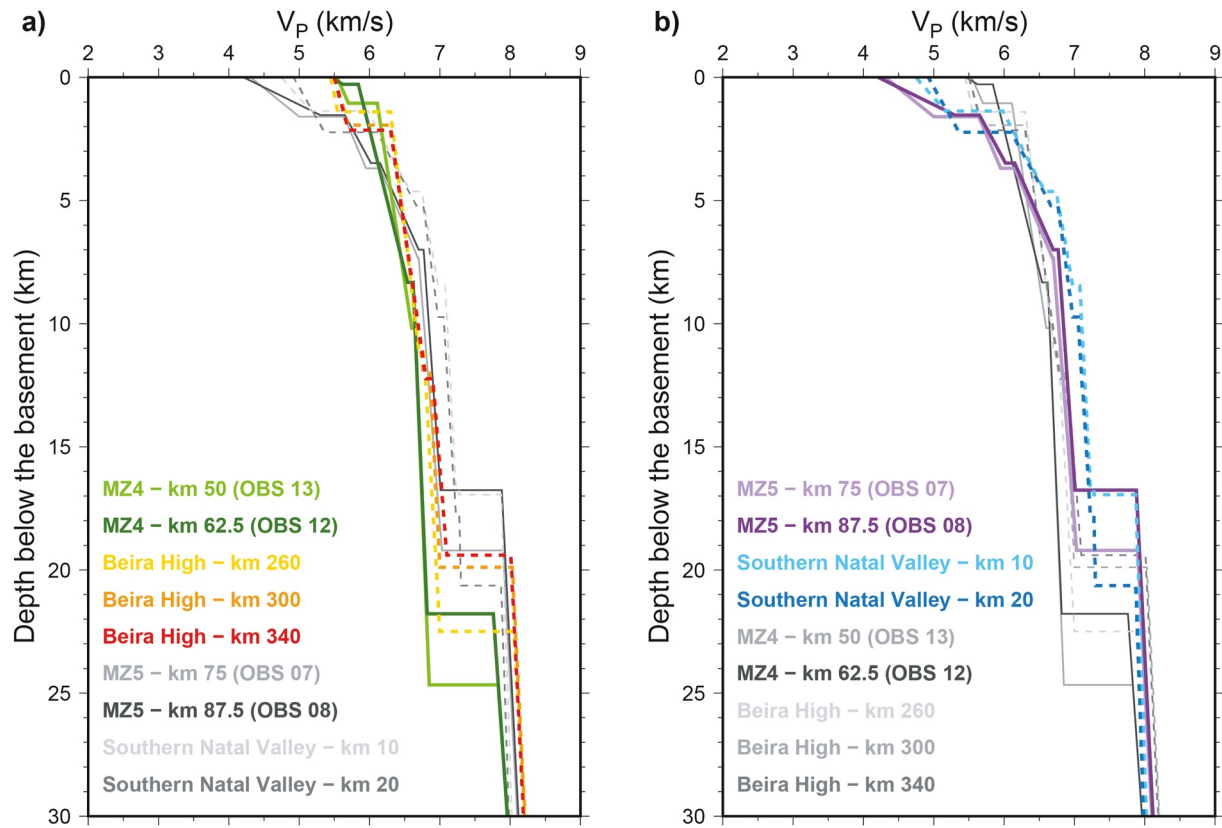


Figure 9. Comparison of vertical velocity profiles in the thinned continental domain with (a) the Beira-High (Mueller et al., 2016) and (b) the Natal Valley (MZ1, Moulin et al., 2020).

top of the acoustic basement also shows strong amplitude reflectors (2.5–3 s twtt, Figures 7 and 8) at the eastern edge of the continental domain (~60 km in Figure 7a and ~70 km in Figure 8a), and at the top of the western large half-graben (10–40 km in Figures 7a and 20–50 km in Figure 8a). These reflectors, located at the top of an erosional surface and at the base of the post-rift sequence, probably indicate a layer rich in volcanic material (Figures 7a and 8a).

Seismic velocities in the crustal layers range from 5.9 to 7.0 km/s along MZ4 and from 5.5 to 7.5 km/s along MZ5, which probably includes some compacted sediments (Figures 5 and 6). As comparisons, the seismic velocities in the thinned continental crust of profile MZ4 are similar to those of the thinned continental crust in the Beira High profiles (Figure 9a; Mueller et al., 2016) and velocities of the thinned continental crust in profile MZ5 are similar to velocities of thinned continental crust in the Southern Natal Valley (Figure 9b; Leprêtre et al., 2021; Moulin et al., 2020). The maximum crustal thickness onshore is approximately 35 km along both profiles (Figures 5 and 6). These characteristics suggest the presence of continental crust with probable magmatic additions below the Mozambique Coastal Plain along MZ5 (see discussion on magmatism).

The average crustal thinning is similar along both profiles: Moho depth decreases by 25.5 km over 160 km in MZ4 as the crust thins from 33 to 9.5 km, sediments excluded (Figure 5) and Moho depth decreases by 25.5 km over 150 km in MZ5 as the crust thins from 35 to 11.5 km (Figure 6), with an average thinning of 0.15 km/km (average interface dip $<10^\circ$). However, the geometry of the necking is different in the two profiles. The Moho in MZ4 rises mostly by steps (model distances of –40, 50, and 95 km, Figure 5) while the rise is more continuous in MZ5 (Figure 6). MZ4 shows two basement highs at model distances of 60 and 85 km. These basement highs are located above a zone where the mid-crustal reflector shows a complex geometry as well as major kinks in the Moho discontinuity (Figure 5a). This Moho geometry and associated basement highs correspond to the crustal necking zone for line MZ4 (Figure 5), and similar basement highs are located at the seaward limit of the continental crust along line MZ5 (Figure 6). These basement highs are marked by magnetic anomalies in both profiles, implying a magnetic contrast between sedimentary and crustal structures (Figures 5a and 6a). The free-air

gravity anomaly decreases toward the east in the continental domain and is lowest at the continental-transitional domain boundary, which is consistent with the geometry of the crustal structures, similarly to the “edge effect” as described and modeled by Watts (2001) across the Beira High margin. Seismic reflection lines highlight a series of normal faults through these basement highs forming tilted blocks and thick volcano-sedimentary basins (Figures 7 and 8; Roche et al., 2021). Most of the normal faults dip eastward, toward the oceanic domain. The fault with the largest vertical offset is located at the western extremity of the seismic reflection lines and controls the thick volcano-sedimentary wedge (up to 4 s twt).

4.2. The Oceanic Domain

Average P-wave velocity model in the oceanic domain consists of the water column, four or five sediment layers, three crustal layers, and one mantle layer (Figures 5 and 6). The oceanic crust is defined as three layers along both lines. The first layer shows thicknesses of 1.0 ± 0.3 km for MZ4 and a more variable of 1.1 ± 0.6 km along MZ5. The thicknesses of the second layer are 1.5 ± 0.3 km and 2.5 ± 0.3 km along MZ4 and MZ5, respectively. The third layer shows the lowest velocity gradients as well as the largest difference in thickness between the two profiles: MZ4 layer thickness is 6.5 km while MZ5 layer thickness is 9–11 km. The velocities of the MZ4 oceanic crustal layers range from 5 to 5.4, 6.1–6.7, and 6.9–7.1 km/s in the three layers, from top to bottom. MZ5 crustal layers show slightly higher velocities from 5 to 6, 6–6.9, and 6.9–7.15 km/s. These three layers correspond to the typical oceanic layering with velocity ranges similar to values observed along oceanic crusts of similar age (Figure 8a). Thus, the oceanic domain is characterized by an 8–9 km and 9–13 km thick crust along MZ4 and MZ5, respectively (Figures 5 and 6). Such crustal thicknesses are larger than typical oceanic crust. Indeed, the “normal” oceanic crust we use in Figure 10a corresponds to a compilation of vertical velocity profiles of oceanic crust in the Atlantic with ages similar to those expected in our study area (White et al., 1992). However, the Atlantic-type oceanic crust shows little or no excess magmatic activity beyond that of normal oceanic crust formation (Cannat et al., 2006; Escartín et al., 2008). The velocities in the oceanic domain are most comparable to velocity structures of oceanic crust that have been affected by mantle plumes (Figure 10b; Schimschal & Jokat, 2018; White, 1992). Thus, the greater thickness of the oceanic crust here is most probably due to late-stage intensive magmatic activity.

The top of the oceanic basement shows rough morphology in profile MZ5, with clear basement highs, while the top of oceanic basement in profile MZ4 shows very limited roughness (Figures 6c and 7c). The series of basement highs along MZ5 may be interpreted as buried volcanic seamounts (Figure 8c, blue arrows, model distances of 210, 225, 240, and 255 km). Indeed, we observe a series of strong reflections within the sediment column (red arrows in Figure 8c) on both sides of each seamount, where the seismic velocities are higher than in the surrounding/unaffected sediments. Velocities jump from the typical ~ 2 to 2.5–3 km/s just above these strong reflections. This implies the presence of some volcanic material such as lava-flows or sills interstratified within the sedimentary sequence. The sediment/magmatic reflectivity shows some top-laps on each side of the buried seamounts, indicating that these seamounts were emplaced after the onset of steady-state seafloor spreading (Figure 8c). Furthermore, the magnetic anomalies are highly variable along MZ5 (Figure 6), highlighting basement features, interpreted as volcanic seamounts (Figure 8c). The magnetic signal also shows a strong increase at the easternmost end of MZ4 (Figure 5), which may be related to an off-profile volcano, perhaps one of the Neogene volcanoes (Figure 1b). Similarly, the free-air gravity anomaly in the oceanic domain shows variations above the seamounts along MZ5 whereas it is continuous along MZ4, which is consistent with the continuous top basement and modeled oceanic layers (Figures 5 and 6).

A clear series of dipping reflectors are also observed in the oceanic crust along MZ4 (Figure 7c, intra-crustal reflections, highlighted in purple in the top panel). Similar features were observed in seismic profiles on other oceanic crusts (e.g., Bécel et al., 2015; Momoh et al., 2017; Sauter et al., 2021). These can be related to magmatic layering or shear zones that are crossed with a slight angle compared to the oceanic crust fabric.

4.3. The Transform Zone

Within the transform zone, we observe more intense faulting and magmatic activity. In particular, the velocity model along MZ5 shows a lot of variations in the upper-crustal structures, which may be related to more intense faulting (Figure 6, km 95–145, 5–10 km depth). The top of the crust in both profiles is slightly deeper (<500 m).

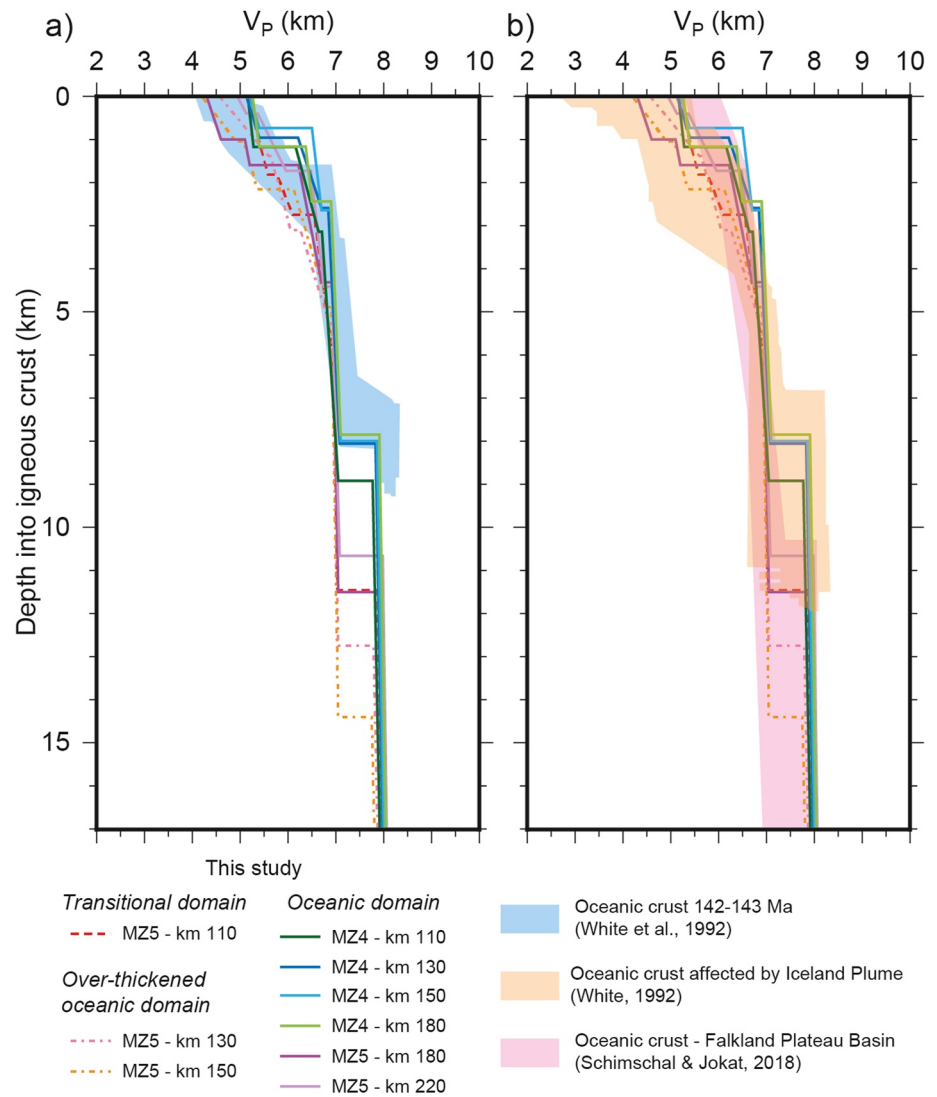


Figure 10. Comparison of vertical velocity profiles with previously published studies. Dashed lines correspond to profiles in the transitional and over-thickened oceanic domains and continuous lines correspond to the oceanic domain. (a) Comparison with various vertical velocity profiles in oceanic crusts of similar ages in the Atlantic (White et al., 1992). (b) Comparison with various vertical velocity profiles in oceanic crust affected by mantle plumes (Schimschal & Jokat, 2018; White, 1992).

in the transform zone than in the oceanic domain further east (Figures 5 and 6). In this zone, complex structures resulting from intense faulting and magmatic activity are clearly delineated by high-resolution seismic data (Figures 7 and 8b). We observe a series of reflectors dipping toward the east at the top of basement along both profiles (model distances of 120–140 km, Figures 6b and 130–150 km, Figure 7b). The reflectivity of these structures is sharp, with strong amplitudes and low-frequency reflectors, indicative of divergent geometries such as seaward dipping reflectors (SDRs), volcanic units, or volcanoclastic sedimentary units.

4.3.1. The Over-Thickened Oceanic Domain

The P-wave velocities along profile MZ4 show very smooth crustal layering in the transform domain, typical of oceanic crust, while the velocity scheme of the transform domain basement along MZ5 shows an additional layer compared to the oceanic crust observed further east (Figure 8, km 85–140), and a much thicker crust (up to 14.5–150, Figure 6). We modeled this layer the same as the top basement layer in the continental domain. However, velocities increased from 5.4 to 5.9 km/s in the continental domain to 5.7–6.1 km/s beneath OBS 10 (km 110; Figure 6). In addition, we observe a lateral interruption of this layer at 110 km, with an area of high P-wave velocities (>6.6 km/s, Figures 6a and 8b). This extra layer may be due to the presence of some volcanic

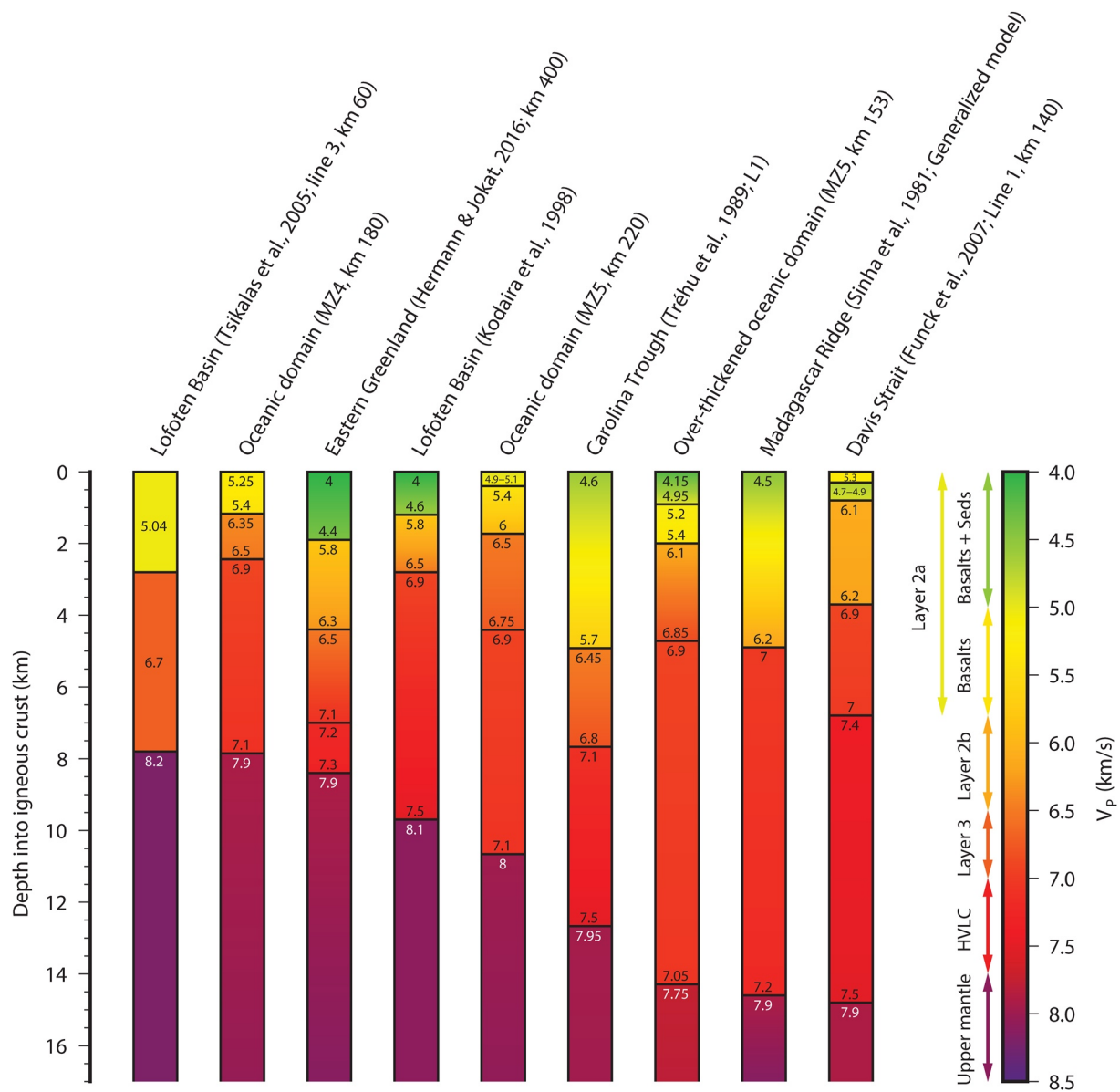


Figure 11. Comparison of 1D P-wave velocity-depth structures in the crust at representative locations along MZ4 and MZ5 with oceanic crust models from previously published studies that have experienced varying amounts of magmatic activity (Funck et al., 2007; Hermann & Jokat, 2016; Kodaira et al., 1998; Sinha et al., 1981; Tréhu et al., 1989; Tsikalas et al., 2005).

material from a magmatic episode that happened at the end of the shear stage, as it appears just where the crust is the thinnest. Furthermore, the reflectivity beneath the acoustic basement is sharp and shows high amplitudes, similarly to the signal observed on each side of the seamounts in the oceanic domain (Figure 8b). Indeed, the crust at model distances of 115–175 km along MZ5 is thicker than the oceanic crust observed further east, but the crustal layering is very similar (Figures 6, 8b, 8c, and 10). This thicker crust is comparable to the Madagascar Ridge crust, interpreted as thickened oceanic crust affected by a mantle plume (Figure 11, Sinha et al., 1981). Thus, as seismic velocities in this area are similar to the velocities observed further east (Figure 6a), and there are clear indications of extensive magmatic activity in this area, perhaps this zone is overthickened oceanic crust that experienced large amounts of intensive magmatic activity.

4.3.2. The Transitional Domain

The transitional domain consists of the domain located between the continental and oceanic domains. It is included in the transform zone, and therefore is affected by the transform movement. These domains and zone are defined in Figures 5 and 6. The transitional domain corresponds to the area where the nature of the crust is unclear, the passage from clear thinned continental crust to the oceanic crust (over-thickened or not). This domain is bordered on the west by a major fault, clearly visible on both profiles (Figures 7a and 8a), which corresponds to the westernmost strand of transform fault zone (Figure 1b). Further east within the transform zone is an area where the acoustic basement dips toward the ocean (MZ4, Figures 5a and 7b) or to a zone where the layer defining part of the upper continental crust layer continues toward the ocean (beneath OBS09 and 10, Figure 6a). Thus, the nature of this domain is still uncertain as both continental and oceanic crusts can explain the structures, which may have been affected by intense faulting and intense magmatic activity.

4.4. Uppermost Mantle Velocities

Uppermost mantle P-wave velocities can be as low as 7.5 and 7.8 km/s at the seaward termination of the necking zone along MZ4 and MZ5, respectively (Figures 5 and 6). MZ5 also shows lower velocities (7.7 km/s) further east, where the crust is thicker than in the adjacent parts of the profile (Figure 6, beneath OBS 13). This is lower than the expected velocities in the uppermost mantle (>7.8 km/s; Christensen & Mooney, 1995). We discuss the processes which might lead to such velocities in Section 5.1.

5. Discussion

5.1. Magmatism

Evidence of magmatic activity are omnipresent in the study area (Figures 7 and 8). A major difference in the magmatic activity between the two profiles is apparent in the oceanic crust: MZ5 shows a series of large buried seamounts as well as a much thicker layer 3 than MZ4 (7–9.5 km vs. 5–5.5 km, Figures 5, 6, 7c, and 8c). The velocity-depth profiles of the oceanic crust of MZ4 are on the thicker end of the typical range oceanic crust thickness (White et al., 1992, Figure 10a). These thicknesses are comparable to oceanic crust in vicinity of a mantle plume (e.g., Iceland Plume; Figure 10b; White, 1992). The thickness of the oceanic crust along MZ5 is even greater (up to 14.5 km, Figure 10). It shows similarities with the oceanic crust of the Falkland Plateau Basin, which is an oceanic plateau with crust up to 20 km thick emplaced in the vicinity of a regional thermal anomaly (Schimschal & Jokat, 2018, Figure 10b). The oceanic crustal layering along MZ4 and MZ5 is similar to that of oceanic crust at magmatic rifted margins such as the Lofoten Basin in Eastern Greenland (Figure 11; Kodaira et al., 1998; Tsikalas et al., 2005; Hermann & Jokat, 2016). This is unexpected as the spreading half rates for the formation of this oceanic crust are approximately 8.3 mm/yr in the time frame of M25 to M0r (Mueller & Jokat, 2019), which is at the lower end of the range of seafloor spreading rates. At such slow spreading rates, one would expect thin, irregular, and faulted oceanic crust, to form (e.g., Cannat, 1996). However, the mafic Layer two of the oceanic crust in our study area is continuous, which is consistent with steady-state melt production at intermediate and fast-spreading rates. Some complex reflectivity is observed beneath the P_mP reflections (e.g., Figure 4d, sets of reflected arrivals beneath the picked P_mP , in orange, clearly visible on the right branch of the record), which is characteristic of high velocity lower crust. We could not model such a feature as a unique solution. Similar reflectivity is also observed in the uppermost mantle in the oceanic domain of MZ4 (Figure 7c, annotated as “deep strong reflectors”). In any case, these features may be interpreted as a magmatic contribution and additions at the base of and in the crust.

In the continental domain, there are indications of high velocities at the base of the continental crust along MZ5 (Figure 6, $V_p > 7.2$ km/s, up to 7.5 km/s). Although this area of the model is characterized by less well-constrained velocities because the seismic rays traveled in only one direction, it is clear that the velocities at the base of the continental crust along MZ5 are higher than those along MZ4. Such a high-velocity lower crust, is either interpreted as magmatic underplating or intrusions in the lower crust (e.g., Bauer et al., 2000). Here, a large landward dipping volcano-sedimentary wedge overlays the continental crust (Figures 7a and 8a). This implies diking of igneous material through the thinned continental crust as well as basin filling with magmatic material. Further offshore, similar processes are observed with magmatic additions at the top of the transitional crust as well as the oceanic crust of the transform zone.

P-wave velocities in the uppermost mantle are generally in the expected range of 7.8–8 km/s. However, these velocities are lower than normal under the thinned continental and transitional crust along MZ4 (Figure 5, model distances of 50–100 km) and under the overthickened oceanic crust along MZ5 (Figure 6, model distances of 120–180 km). Such low velocities in the uppermost mantle overlain by thin crust might indicate an abnormally hot mantle or magmatic underplating at the base of the crust (e.g., Hirsch et al., 2009; Minshull et al., 2008). Small-scale convection due to the varying lithospheric thickness on either side of the transform faults might be invoked as previously proposed, for example, in the Gulf of Aden (Korostelev et al., 2015), to explain low seismic velocities in the lithospheric mantle. The presence of a large mantle plume imaged from South Africa to Afar (e.g., O'Connor et al., 2019) could also explain such velocities. Elevated temperatures in the mantle (140–170°C, e.g., O'Connor et al., 2019) could account for ~100 m/s of the velocity anomaly (e.g., Xu et al., 2008). While a mineralogical variation as small as 0.51% (e.g., Cammarano et al., 2003) is enough to explain large modeled temperature differences, and thus, the rest of the velocity anomaly. The mantle plume hypothesis may better explain these low velocities in the magma-rich context of the upper mantle.

We consider two main hypotheses to explain such widespread magmatism, which is strongly variable in time and space. The first hypothesis is that the transform margin was affected by a major melting anomaly in the mantle during its formation and evolution. The more extensive magmatic activity toward the south is in agreement with the location and timing of the mantle plume proposed by White and McKenzie (1989) as a 1000-km diameter feature, centered beneath the Natal Valley south of our study area. The second hypothesis simply involves the segmentation and transform the movement of the oceanic crust. The oceanic crust in the transform is over-thickened. This may be due to motion on the transform fault bringing the eastern segment of the mid-ocean ridge next to the cooler, older oceanic crust such that thicker crust was produced by the spreading center. This is consistent with the estimated early Cretaceous age of the Mozambique Ridge (e.g., Erlank & Reid, 1974; Jacques et al., 2019; König & Jokat, 2010; Thompson et al., 1982), which is a highly magmatic structure at the southward extension of the transform zone of MZ4 and MZ5 (Figure 1). Thus, the second hypothesis may provide a good explanation to the locally thick oceanic crust along MZ5 while the first hypothesis may explain the widespread magmatism in the continental domain.

5.2. Crustal Structure and Transform Margin Evolution in a Magma-Rich Context

Our two P-wave velocity models confirm the continental nature of the South Mozambique Coastal Plain, which represents the pre-rift crust in Mozambique (landward part of our profiles, Figures 5 and 6). Its initial thickness is at least 30 km according to gravity studies in the area (Gwavava et al., 1992). Our results show a crustal thickness of up to ~35 km along MZ5 (Figure 6), and up to 41 km in refraction profiles in Natal Valley (Leprière et al., 2021; Moulin et al., 2020). A joint inversion of receiver functions and surface wave dispersion curves shows crustal thicknesses of ~36–40 km in the Eastern Kaapval craton (see Figure 1 for location; Kgaswane et al., 2009). Such a highly oblique rifting context is usually characterized by transfer or accommodation zones that allow for the juxtaposition of continental and oceanic crusts (Figure 12a). We interpret the transform zone in the study area as a system of faults with extensive indications of magmatic activity (magmatic infilling, over-thickened oceanic crust, low velocity mantle) that separates the thinned continental domain from the oceanic domain. We propose that the continental crust of the Limpopo segment underwent oblique extension that evolved into a transform stage. Thus, the Limpopo segment represents a transform margin associated with significant magmatic activity.

The presence of over-thickened oceanic crust along MZ5 and a wide zone affected by the transform motion and excess magmatic activity concurs in the absence of a distinct marginal ridge along MZ4 and MZ5. The formation of a marginal ridge is expected along with thermal uplift, both effects created by the migration of an oceanic spreading center along the edge of the continental crust (e.g., Basile, 2015; Mercier de Lépinay et al., 2016). The transform fault system experienced both strike-slip and some extension (Figure 2), resulting in a wide zone of deformation (40–50 km) that was affected by magmatic activity, that is, a leaky transform. Thus, the sharp thermal gradient between the oceanic spreading center and the cool continental crust that is expected to create a marginal ridge did not happen here. We propose that the Limpopo margin went through an episode of uplift marked by an erosional surface observed in the western part of the profiles (Figures 7a and 8a), which affected the acoustic basement. This uplift may be related to the presence of a long-term mantle plume responsible for several specific periods of magmatic activity (183 Ma to present day; e.g., Torsvik et al., 2006).

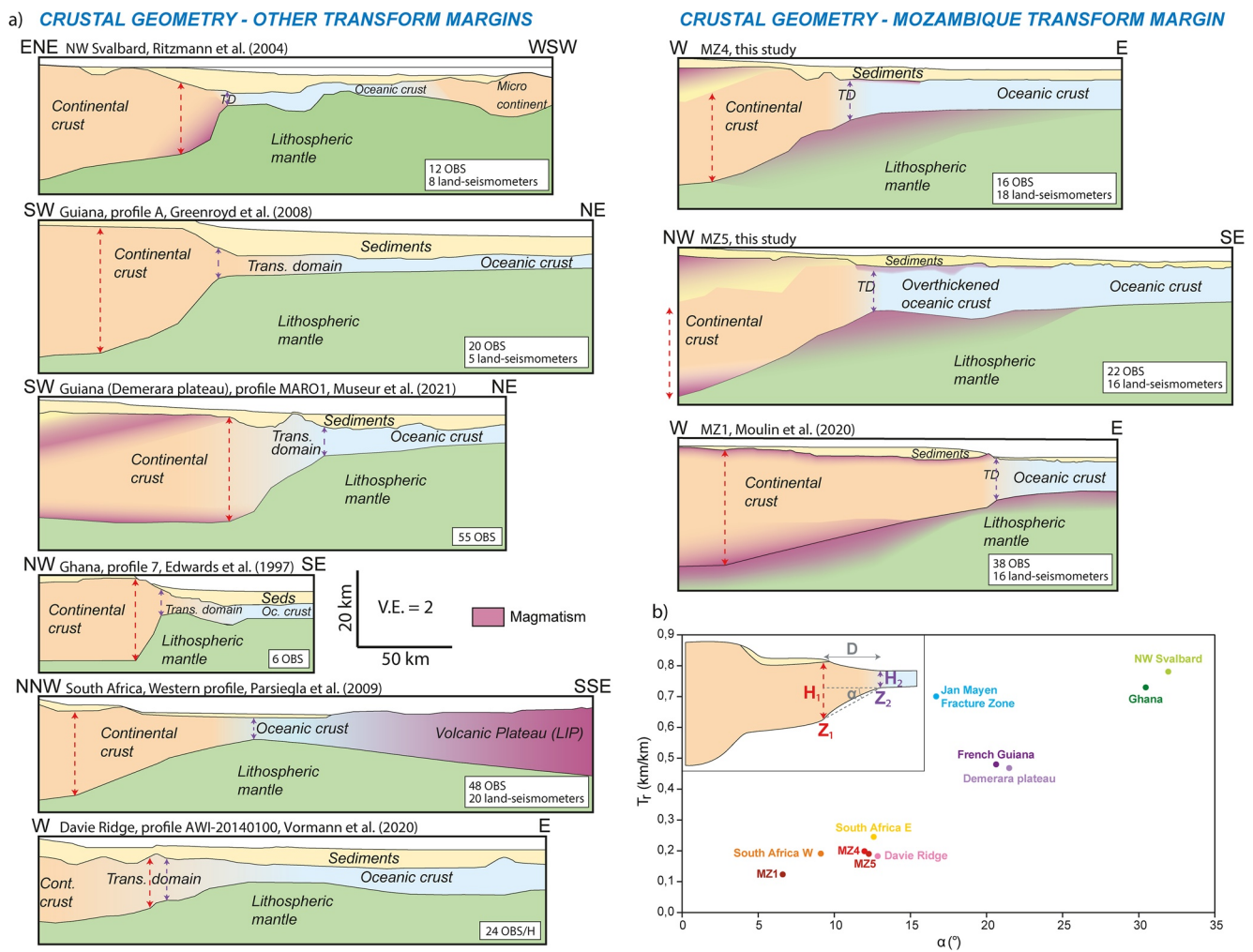


Figure 12. Comparison of the crustal structures of the Mozambique transform margin with other known transform margins. (a) Simplified crustal structures across NW Svalbard, Guiana, Ghana, and South Africa transform margins (Edwards et al., 1997; Greenroyd et al., 2008; Museur et al., 2021; Parsieglia et al., 2009; Ritzmann et al., 2004; Vormann et al., 2020) compared with the structures observed along the sections from the Mozambique transform margin (Moulin et al., 2020; this study). The red and purple arrow refer to the measurements used in Table 4 and panel (b). (b) Diagram showing T_r (crustal thinning ratio, i.e., vertical km for each horizontal km) as a function of α (dip of the Moho), both corrected for the angle of the profile with the trend of the considered transform. Details of how these values were calculated are presented in Table 4.

Thermo-mechanical models predict the formation of some deep basins, perpendicular to the future transform zone, followed by the formation of basins parallel to the transform zones after 20 Myr of activity (Le Pourhiet et al., 2017). In the Limpopo margin, only basins parallel to the trend of the transform are imaged. These basins should correspond to a later stage of the transform fault development. A large N-S trending basin near the coast shows syn-tectonic infilling (“Landward dipping reflectors,” Figures 7a and 8a), which we think is a long-lived sedimentary basin. Active since the permo-trias rifting stage (Basin 1, Figures 7a and 8a), this basin was reactivated during the Early Jurassic rifting event (Basin 2, Figures 7a and 8a), which resulted in the formation of the northern Beira-High and Angoche margins, before the onset of seafloor spreading. During this latter stage, the extension localized along the future transform boundary with the emplacement of volcanism, observed as magmatic infill (see Figure 2, stages TF1 to TF3, and Figures 7a and 8a). The presence of magmatic activity throughout its history clearly indicates that the Limpopo transform margin is a magma-rich transform margin.

Table 4

Geometry of the Crustal Thinning Along the Transform Fault for a Variety of Transform Margins, Including Different Tectono-Magmatic Evolutions

Margin/Profile	Summary of tectono-magmatic history	θ (°)	Crustal thicknesses (km)		Moho depths (km)		D (km)	α (°)	T_r (km/km)
			H_1	H_2	Z_1	Z_2			
Mozambique ^a (23.5°S)/MZ4	Oblique rifting + Transform stages. Volcanism: syn-rift, syn- and post-transform.	90	24	9.5	32.5	17	73	12.0	0.20
Mozambique ^a (25°S)/MZ5	Oblique rifting + Transform stages. Volcanism: syn-rift, syn- and post-transform.	70	32	11.5	41	17.5	115	12.3	0.19
Mozambique ^b (27°S)/MZ1	Oblique rifting + Transform stages. Volcanism: syn-rift, syn- and post-transform.	80	26	9	32	16	140	6.6	0.12
Davie Ridge ^c (14.5°S)/AWI-20140100	Oblique rifting + Transform stages. Some post-transform volcanism further south.	85	13	11	19	16.5	11	12.9	0.18
South Africa ^d (23.5°E)/AWI-20050100-FRA	Rifting + Transform stages. Pre-rift (Karoo), syn-transform (marginal ridge) and post-transform (Agulhas Plateau) volcanism.	85	15.5	6	20	12	50	9.1	0.19
South Africa ^e (25°E)/AWI-20050200-GRA	Rifting + Transform stages. Pre-rift (Karoo), syn-transform (marginal ridge) and post-transform (Agulhas Plateau) volcanism.	70	21	9.5	26	15.5	50	12.6	0.24
Jan Mayen Fracture Zone ^f /AWI-94340 & AWI-20090100	Two rifting events + transform stages. Iceland Plume during the second rifting event (3 km thick HVLC), excess magma production at the leaky fracture zone.	30	21	7	19	13	40	16.7	0.70
French Guiana ^g /Profile A	Leaky transform but no syn-tectonic volcanism identified.	75	33	7.5	35	15	55	20.6	0.48
Demerara plateau ^h /MAR01	Rift + Transform stages. Syn-rift volcanism (HVLC + igneous material overlaying the plateau).	70	26.5	4.5	33.5	15	50	21.5	0.47
Ghana ⁱ /Profile 7	No clear evidence of igneous material (but not excluded), maybe leaky transform stage.	75	20	4.5	23	10.5	22	30.5	0.73
NW Svalbard ^j /AWI-99400	Syn-transform magmatism (HVLC) due to mid-ocean ridge migration along the thick continental crust.	60	17	0.1	23.5	10	25	31.9	0.78

Note. θ is the angle of the profile orientation relative the transform fault zone. Crustal thicknesses (H) and Moho depths (Z) are measured to highlight the oceanward-most crustal thinning near the transform fault, where the thinning is most intense. H_1 and Z_1 are measured in the thinned continental domain, just landward of where thinning begins. H_2 and Z_2 are measured at the thinnest continental crust. D refers to the horizontal distance, along the profile, from points 1 to 2. We define α as the dip of the Moho interface: $\alpha = \tan^{-1} \left(\frac{Z_1 - Z_2}{D \cos(90 - \theta)} \right)$, and T_r the crustal thinning ratio: $T_r = \frac{H_1 - H_2}{D \cos(90 - \theta)}$, between 1 and 2, both corrected for the profile orientation relative to the transform (θ). References:

^aThis study. ^bMoulin et al. (2020). ^cVormann et al. (2020). ^dStankiewicz et al. (2008). ^eParsieglia et al. (2009). ^fHermann & Jokat (2016). ^gGreenroyd et al. (2008). ^hMuseur et al. (2021). ⁱEdwards et al. (1997). ^jRitzmann et al. (2004).

5.3. Comparison With Known Transform Margins

A comparison of the crustal geometries of other transform margins (Figure 12 and Table 4) shows more even thinning of the crust along MZ4 and MZ5 than found at some other transform margins (e.g., NW Svalbard, Guiana, and Ghana; Edwards et al., 1997; Ritzmann et al., 2004; Greenroyd et al., 2008). Another important difference between the Mozambique transform margin and some other transform margins is that the oceanic crust along MZ4 and MZ5 is thicker: 9–14.5 km thick. The other transform margins in this comparison tend to have thinner than the typical 5–7-km-thick oceanic crust (Figure 12a; e.g., Edwards et al., 1997; Ritzmann et al., 2004; Greenroyd et al., 2008). The oceanic crust south of our study area is also thicker than might be expected (Figure 12a; Moulin et al., 2020), which is consistent with the intensive magmatic activity evident during margin formation (see Section 5.1). South Africa transform margin, with thicker than typical oceanic crust associated with the Agulhas LIP, is the one exception (Parsieglia et al., 2009).

Most of these margins show indications that magmatic activity affected their continental crust at various stages of margin formation. The Demerara continental crust shows some indications of magmatic underplating or lower crustal intrusions, evident as a clear double wide-angle reflection, as well as extensive igneous material overlaying the plateau (e.g., Museur et al., 2021; Reuber et al., 2016). The SW Svalbard lower continental crust was intruded by igneous material when the oceanic ridge migrated along the thick continental crust during the

evolution of the transform zone (Ritzmann et al., 2004). Only the Ghana profile does not show clear evidence of magmatic additions (Edwards et al., 1997).

A comparison of the continental crustal thinning geometries within the outer continental domains of several transform margins is presented in Figure 12. Outer continental domains are delimited on one side by the necking line and on the other side by the thinnest crust near the transform (see inset in Figure 12b). Comparing the outer continental domain from one margin to another allows us to help distinguish extensional deformation (i.e., eventual pre-transform rifting episodes that may have thinned the crust further onshore; see Table 4, summary of tectono-magmatic history column) from shear deformation. Figure 12b presents a graphic representation of the variations of the crustal thinning ratio (T_r) as a function of the dip of the Moho interface (α) within the outer continental domain (see the caption of Table 4 for explanation parameters and their calculation). The points, with one exception, fall along what could be interpreted as a trend that predicts that the dip of the Moho is related directly to the crustal thinning ratio. The Jan Mayen Fracture Zone is the exception to this trend, perhaps due to the fact it was affected by two phases of rifting that thinned the continental crust significantly before transform development (Hermann & Jokat, 2016).

The cluster of the majority of points on the T_r versus α indicates that transform margins tend to have relatively narrow outer continental domains and very shallow to intermediate Moho dips. Narrow outer continental domains and shallow Moho dips may seem counterintuitive until the fact that these domains at these margins tend to end abruptly in transform fault or transform fault systems is taken into consideration. Shallow Moho dip may be one effect of the magmatic activity that these margins experienced during formation. However, magmatic activity such as volcanism, emplacement of igneous bodies, and underplating tends to thicken the crust, the inverse of what we observe. This may be an indication that while magmatic activity smooths and flattens the Moho, factors such as inherited topography and structures, stretching and faulting during an extensional stage of margin development, and syn-tectonic sedimentation, all of which are evident in the Limpopo Margin MZ4 and MZ5 profiles, may also play an important, if not dominant, role in continental crustal thinning. Characteristics of continental crustal thinning observed at the Limpopo Margin are similar to those found in seismic profiles along the eastern coast of Africa as far north as the Davie Ridge and as far south as South Africa, suggesting that this transform margin underwent (a) trans-tensional deformation during its early stage(s) and (b) intense and extensive magmatic activity during all stages of the margin evolution.

One suggestion for further studies would be to acquire seismic refraction data at the conjugate margins of the locations of the points in the cluster to determine if they have matching crustal thinning characteristics. Additionally, the duration of margin evolution before the final stage transform motion development could be used to weight the crustal thinning ratio.

6. Conclusions

The layered models of two crustal scale wide-angle seismic refraction data and the interpretation of industry and academic seismic reflection data across the magma-rich Limpopo transform margin were processed and examined to produce the following series interpretations and conclusions regarding (a) the delineation of the different crustal domains, as well as a transform zone, (b) the identification of magmatic features along the whole margin, which occurred at all stages of the formation and evolution of the margin, and (c) the study of the structures and geometry at crustal scale and comparison of these structures with those found at other margins across the world.

The P-wave velocity models and coincident seismic reflection profiles highlight distinct crustal domains and associated indications of magmatic activity:

- 1) The Mozambique Coastal Plain is underlain by continental crust, which is at least 25 km thick. The crust thins by 23.5 km over a distance of 150–160 km and is overlain by a >10-km thick volcano-sedimentary infilled basin that indicates the occurrence of a rifting phase before the transform movement, associated with some magmatism.
- 2) The oceanic domain is defined by 8–14.5 km thick oceanic crust that shows a continuous typical layering, which is unexpected in this context of ultra-slow spreading rates (8.3 mm/yr). This attests to intense magmatic activity during the formation of the oceanic crust.

- 3) We define a transform zone that extends from the thinned continental domain to the oceanic domain and that displays evidence of intense faulting and magmatic activity (i.e., seaward dipping reflectors). Indeed, the Limpopo transform zone was a system of faults that were active during the trans-tensional stage of margin evolution.
- 4) The uppermost mantle shows low P-wave velocities (7.5–7.8 km/s), which may be explained by the influence of a thermo-chemical mantle anomaly.

The intense magmatic activity that affects the structures of the Limpopo transform may be explained by the combination of two magmatic processes:

- 1) A deep-seated melting anomaly, which is active since at least the early Jurassic period, is at the origin of the volcano-sedimentary wedge overlying the continental crust and the thick oceanic crust.
- 2) The thicker oceanic crust and excess magmatic activity in the transform zone is also due to the effect of the trans-tensional movement along the transform, which led to a leaky transform phenomenon. This is consistent with the presence of the Mozambique Ridge to the south, which is mostly volcanic in nature.

The quantification of the crustal thinning across several transform margins across the world shows a probable relationship between the geometry of the crust next to the transform and its thermal and/or structural history. In particular, the crustal thinning across the transform margins of Mozambique and South Africa show similar characteristics. However, further studies are essential to bring better insights or explanations for such observation.

Data Availability Statement

Seismic data sets of the PAMELA-MOZ3 (Moulin & Aslanian, 2016) and PAMELA-MOZ5 (Moulin & Evain, 2016) cruises are archived and referenced in Ifremer SISMER database and can be requested at <https://doi.org/10.17600/16009500> and <https://doi.org/10.17600/16001600>. The picks and final velocity models are provided in RAYINVR format on SEANOE at <https://doi.org/10.17882/76489> (Watremez et al., 2021). GMT was used for Figures 2–7 and 9–10 (Wessel et al., 2013) and Seismic_Un*x was used for Figures 3, 6, 7, and 9 (Stockwell, 1999). Zplot is available from <https://terra.rice.edu/departement/faculty/zelt/zplot.tar.gz>.

References

- Ammann, N., Liao, J., Gerya, T., & Ball, P. (2018). Oblique continental rifting and long transform fault formation based on 3D thermomechanical numerical modeling. *Tectonophysics*, 746, 106–120. <https://doi.org/10.1016/j.tecto.2017.08.015>
- Avedik, F., Renard, V., Allenou, J.-P., & Morvan, B. (1993). “Single bubble” air-gun array for deep exploration. *Geophysics*, 58(3), 366–382. <https://doi.org/10.1190/1.1443420>
- Basile, C. (2015). Transform continental margins—Part 1: Concepts and models. *Tectonophysics*, 661, 1–10. <https://doi.org/10.1016/j.tecto.2015.08.034>
- Basile, C., Mascle, J., Benkheilil, J., & Bouillin, J. P. (1998). 11. Geodynamic evolution of the Côte d’Ivoire-Ghana transform margin: An overview of leg 159 results 1. *Proceedings of the Ocean Drilling Program* (Vol. 159). Scientific Results.
- Bauer, K., Neben, S., Schreckenberger, B., Emmermann, R., Hinz, K., Fechner, N., et al. (2000). Deep structure of the Namibia continental margin as derived from integrated geophysical studies. *Journal of Geophysical Research: Solid Earth*, 105(B11), 25829–25853. <https://doi.org/10.1029/2000JB900227>
- Bécel, A., Shillington, D. J., Nedimović, M. R., Webb, S. C., & Kuehn, H. (2015). Origin of dipping structures in fast-spreading oceanic lower crust offshore Alaska imaged by multichannel seismic data. *Earth and Planetary Science Letters*, 424, 26–37. <https://doi.org/10.1016/j.epsl.2015.05.016>
- Ben-Avraham, Z. C. J. H., Hartnady, C. J. H., & Le Roex, A. P. (1995). Neotectonic activity on continental fragments in the southwest Indian Ocean: Agulhas Plateau and Mozambique Ridge. *Journal of Geophysical Research: Solid Earth*, 100(B4), 6199–6211. <https://doi.org/10.1029/94JB02881>
- Bevington, P. R. (1969). *Data reduction and error analysis for physical sciences*. McGraw-Hill.
- Bird, D. (2001). Shear margins Continent-ocean transform and fracture zone boundaries. *The Leading Edge*, 20(2), 150–159. <https://doi.org/10.1190/1.1438894>
- Blenkinsop, T., & Moore, A. (2013). 5.5 Tectonic geomorphology of passive margins and continental hinterlands. In *Treatise on geomorphology* (pp. 71–92). Elsevier. <https://doi.org/10.1016/B978-0-12-374739-6.00083-X>
- Brune, S., Williams, S. E., & Müller, R. D. (2018). Oblique rifting: The rule, not the exception. *Journal of Geophysical Research: Solid Earth*, 9(5), 1187–1206. <https://doi.org/10.5194/se-9-1187-2018>
- Cammarano, F., Goes, S., Vacher, P., & Giardini, D. (2003). Inferring upper-mantle temperatures from seismic velocities. *Physics of the Earth and Planetary Interiors*, 138(3–4), 197–222. [https://doi.org/10.1016/S0031-9201\(03\)00156-0](https://doi.org/10.1016/S0031-9201(03)00156-0)
- Cannat, M. (1996). How thick is the magmatic crust at slow spreading oceanic ridges? *Journal of Geophysical Research: Solid Earth*, 101(B2), 2847–2857. <https://doi.org/10.1029/95JB03116>
- Cannat, M., Sauter, D., Escartín, J., Lavier, L., & Picazo, S. (2009). Oceanic corrugated surfaces and the strength of the axial lithosphere at slow spreading ridges. *Earth and Planetary Science Letters*, 288(1–2), 174–183. <https://doi.org/10.1016/j.epsl.2009.09.020>

Acknowledgments

The PAMELA project (Passive Margin Exploration Laboratories) is a scientific project led by Ifremer and TOTAL in collaboration with Université de Bretagne Occidentale, Université Rennes 1, Sorbonne Université, CNRS and IFPEN. The authors are thankful to Afonso Loureiro, Carlos Corela and their team, who deployed the onland seismometers for the MOZ3/5 project. The authors offer their profound thanks to Anne Bécel and five anonymous reviewers for their highly constructive and complementary reviews on previous versions of this manuscript. The authors deeply thank Dr. Heather Sloan for post-editing the English style and grammar.

- Cannat, M., Sauter, D., Mendel, V., Ruellan, E., Okino, K., Escartin, J., et al. (2006). Modes of seafloor generation at a melt-poor ultraslow-spreading ridge. *Geology*, *34*, 605–608. <https://doi.org/10.1130/G22486.1>
- Castilla, R., Leroy, S., Moulin, M., Guillocheau, F., Robin, C., Lescanne, M., et al. (2015). *Structural map of the Mozambique channel*.
- Christensen, N. I., & Mooney, W. D. (1995). Seismic velocity structure and composition of the continental crust: A global view. *Journal of Geophysical Research: Solid Earth*, *100*(B6), 9761–9788. <https://doi.org/10.1029/95JB00259>
- Christeson, G. L., Goff, J. A., & Reece, R. S. (2019). Synthesis of oceanic crustal structure from two-dimensional seismic profiles. *Reviews of Geophysics*, *57*(2), 504–529. <https://doi.org/10.1029/2019RG000641>
- Courgeon, S., Bachèlery, P., Jouet, G., Jorry, S. J., Bou, E., BouDagher-Fadel, M. K., et al. (2018). The offshore east African rift system: New insights from the Sakalaves seamounts (Davie Ridge, SW Indian Ocean). *Terra Nova*, *30*(5), 380–388. <https://doi.org/10.1111/ter.12353>
- Courgeon, S., Jorry, S. J., Jouet, G., Camoin, G., BouDagher-Fadel, M. K., Bachèlery, P., et al. (2017). Impact of tectonic and volcanism on the Neogene evolution of isolated carbonate platforms (SW Indian Ocean). *Sedimentary Geology*, *355*, 114–131. <https://doi.org/10.1016/j.sedgeo.2017.04.008>
- Cox, K. G. (1989). The role of mantle plumes in the development of continental drainage patterns. *Nature*, *342*(6252), 873–877. <https://doi.org/10.1038/342873a0>
- Daly, M. C., Chorowicz, J., & Fairhead, J. D. (1989). Rift basin evolution in Africa: The influence of reactivated steep basement shear zones. *Geological Society London, Special Publications*, *44*, 309–334. <https://doi.org/10.1144/GSL.SP.1989.044.01.17>
- Deville, E., Marsset, T., Courgeon, S., Jatiault, R., Ponte, J. P., Thereau, E., et al. (2018). Active fault system across the oceanic lithosphere of the Mozambique Channel: Implications for the Nubia–Somalia southern plate boundary. *Earth and Planetary Science Letters*, *502*, 210–220. <https://doi.org/10.1016/j.epsl.2018.08.052>
- Duncan, R. A., Hooper, P. R., Rehacek, J., Marsh, J. S., & Duncan, A. R. (1997). The timing and duration of the Karoo igneous event, southern Gondwana. *Journal of Geophysical Research: Solid Earth*, *102*(B8), 18127–18138. <https://doi.org/10.1029/97JB00972>
- Edwards, R. A., Whitmarsh, R. B., & Scrutton, R. A. (1997). The crustal structure across the transform continental margin off Ghana, eastern equatorial Atlantic. *Journal of Geophysical Research: Solid Earth*, *102*(B1), 747–772. <https://doi.org/10.1029/96JB02098>
- Erlank, A. J., & Reid, D. L. (1974). Geochemistry, mineralogy, and petrology of basalts, LEG 25, Deep Sea Drilling Project. *Initial Reports of the Deep Sea Drilling Project*, *25*, 543–551. <https://doi.org/10.2973/dsdp.proc.25.122.1974>
- Escartin, J., Smith, D. K., Cann, J., Schouten, H., Langmuir, C. H., & Escrig, S. (2008). Central role of detachment faults in accretion of slow-spreading oceanic lithosphere. *Nature*, *455*, 790–794. <https://doi.org/10.1038/nature07333>
- Evain, M., Schnürle, P., Leprêtre, A., Verrier, F., Watremez, L., Thompson, J. O., et al. (2021). Crustal structure of the East African Limpopo margin, a strike-slip rifted corridor along the continental Mozambique Coastal Plain and North Natal Valley. *Journal of Geophysical Research: Solid Earth*, *126*(8), 1865–1897. <https://doi.org/10.5194/se-12-1865-2021>
- Fischer, M. D., Uenzelmann-Neben, G., Jacques, G., & Werner, R. (2017). The Mozambique Ridge: A document of massive multi-stage magmatism. *Geophysical Journal International*, *208*(1), 449–467. <https://doi.org/10.1093/gji/ggw403>
- Flores, G. (1984). The SE Africa triple junction and the drift of Madagascar. *Journal of Petroleum Geology*, *7*(4), 403–418. <https://doi.org/10.1111/j.1747-5457.1984.tb00885.x>
- Funck, T., Jackson, H. R., Loudon, K. E., & Klingelhöfer, F. (2007). Seismic study of the transform-rifted margin in Davis Strait between Baffin Island (Canada) and Greenland: What happens when a plume meets a transform. *Journal of Geophysical Research: Solid Earth*, *112*(B4). <https://doi.org/10.1029/2006JB004308>
- Gaina, C., Torsvik, T. H., van Hinsbergen, D. J. J., Medvedev, S., Werner, S. C., & Labails, C. (2013). The African Plate: A history of oceanic crust accretion and subduction since the Jurassic. *Tectonophysics*, *604*, 4–25. <https://doi.org/10.1016/j.tecto.2013.05.037>
- Greenroyd, C. J., Peirce, C., Rodger, M., Watts, A. B., & Hobbs, R. W. (2007). Crustal structure of the French Guiana margin, west equatorial Atlantic. *Geophysical Journal International*, *169*(3), 964–987. <https://doi.org/10.1111/j.1365-246X.2007.03372.x>
- Greenroyd, C. J., Peirce, C., Rodger, M., Watts, A. B., & Hobbs, R. W. (2008). Do fracture zones define continental margin segmentation? – Evidence from the French Guiana margin. *Earth and Planetary Science Letters*, *272*(3–4), 553–566. <https://doi.org/10.1016/j.epsl.2008.05.022>
- Gwawava, O., Swain, C. J., Podmore, F., & Fairhead, J. D. (1992). Evidence of crustal thinning beneath the Limpopo Belt and Lebombo monocline of southern Africa based on regional gravity studies and implications for the reconstruction of Gondwana. *Tectonophysics*, *212*(1–2), 1–20. [https://doi.org/10.1016/0040-1951\(92\)90136-T](https://doi.org/10.1016/0040-1951(92)90136-T)
- Hastie, W. W., Watkeys, M. K., & Aubourg, C. (2014). Magma flow in dyke swarms of the Karoo LIP: Implications for the mantle plume hypothesis. *Gondwana Research*, *25*(2), 736–755. <https://doi.org/10.1016/j.gr.2013.08.010>
- Hermann, T., & Jokat, W. (2016). Crustal structure off Kong Oscar Fjord, east Greenland: Evidence for focused melt supply along the Jan Mayen fracture zone. *Tectonophysics*, *691*, 110–119. <https://doi.org/10.1016/j.tecto.2015.12.005>
- Hirsch, K. K., Bauer, K., & Scheck-Wenderoth, M. (2009). Deep structure of the western South African passive margin – Results of a combined approach of seismic, gravity and isostatic investigations. *Tectonophysics*, *470*(1–2), 57–70. <https://doi.org/10.1016/j.tecto.2008.04.028>
- Huisman, R., & Beaumont, C. (2011). Depth-dependent extension, two-stage breakup and cratonic underplating at rifted margins. *Nature*, *473*(7345), 74–78. <https://doi.org/10.1038/nature09988>
- Jacques, G., Hauff, F., Hoernle, K., Werner, R., Uenzelmann-Neben, G., Garbe-Schönberg, D., & Fischer, M. (2019). Nature and origin of the Mozambique Ridge, SW Indian Ocean. *Chemical Geology*, *507*, 9–22. <https://doi.org/10.1016/j.chemgeo.2018.12.027>
- Jolivet, L., Gorini, C., Smit, J., & Leroy, S. (2015). Continental breakup and the dynamics of rifting in back-arc basins: The Gulf of Lion margin. *Tectonics*, *34*(4), 662–679. <https://doi.org/10.1002/2014TC003570>
- Jourdan, F., Bertrand, H., Féraud, G., Le Gall, B., & Watkeys, M. K. (2009). Lithospheric mantle evolution monitored by overlapping large igneous provinces: Case study in southern Africa. *Lithos*, *107*(3–4), 257–268. <https://doi.org/10.1016/j.lithos.2008.10.011>
- Jourdan, F., Féraud, G., Bertrand, H., Watkeys, M. K., Kampunzu, A. B., & Le Gall, B. (2006). Basement control on dyke distribution in Large Igneous Provinces: Case study of the Karoo triple junction. *Earth and Planetary Science Letters*, *241*, 307–322. <https://doi.org/10.1016/j.epsl.2005.10.003>
- Jourdan, F., Féraud, G., Bertrand, H., Watkeys, M. K., & Renne, P. R. (2007). Distinct brief major events in the Karoo large igneous province clarified by new ⁴⁰Ar/³⁹Ar ages on the Lesotho basalts. *Lithos*, *98*, 195–209. <https://doi.org/10.1016/j.lithos.2007.03.002>
- Kgaswane, E. M., Nyblade, A. A., Julià, J., Dirks, P. H., Durrheim, R. J., & Pasyanos, M. E. (2009). Shear wave velocity structure of the lower crust in southern Africa: Evidence for compositional heterogeneity within Archaean and Proterozoic terrains. *Journal of Geophysical Research: Solid Earth*, *114*(B12). <https://doi.org/10.1029/2008JB006217>
- Klausen, M. B. (2009). The Lebombo monocline and associated feeder dyke swarm: Diagnostic of a successful and highly volcanic rifted margin? *Tectonophysics*, *468*, 42–62. <https://doi.org/10.1016/j.tecto.2008.10.012>

- Klimke, J., Franke, D., Estevão, S. M., & Leitchenkov, G. (2018). Tie points for Gondwana reconstructions from a structural interpretation of the Mozambique Basin, East Africa and the Riiser-Larsen Sea, Antarctica. *Journal of Geophysical Research: Solid Earth*, 9(1), 25–37. <https://doi.org/10.5194/se-9-25-2018>
- Kodaira, S., Mjelde, R., Gunnarsson, K., Shiobara, H., & Shimamura, H. (1998). Structure of the Jan Mayen microcontinent and implications for its evolution. *Geophysical Journal International*, 132(2), 383–400. <https://doi.org/10.1046/j.1365-246x.1998.00444.x>
- König, M., & Jokat, W. (2010). Advanced insights into magmatism and volcanism of the Mozambique Ridge and Mozambique Basin in the view of new potential field data. *Geophysical Journal International*, 180, 158–180. <https://doi.org/10.1111/j.1365-246X.2009.04433.x>
- Korenaga, J., Holbrook, W. S., Kent, G. M., Kelemen, P. B., Detrick, R. S., Larsen, H. C., et al. (2000). Crustal structure of the southeast Greenland margin from joint refraction and reflection seismic tomography. *Journal of Geophysical Research: Solid Earth*, 105(B9), 21591–21614. <https://doi.org/10.1029/2000JB900188>
- Korostelev, F., Leroy, S., Keir, D., Ahmed, A., Boschi, L., Rolandone, F., et al. (2015). Upper mantle structure of the southern Arabian margin: Insights from teleseismic tomography. *Geosphere*, 11, 1262–1278. <https://doi.org/10.1130/GES01159.1>
- Le Pichon, X., & Hayes, D. (1971). Marginal offsets, fracture zones, and the early opening of the North Atlantic. *Journal of Geophysical Research: Solid Earth*, 76, 6283–6293. <https://doi.org/10.1029/JB076i026p06294>
- Le Pouchet, L., May, D. A., Huille, L., Watremez, L., & Leroy, S. (2017). A genetic link between transform and hyper-extended margins. *Earth and Planetary Science Letters*, 465, 184–192. <https://doi.org/10.1016/j.epsl.2017.02.043>
- Leinweber, V. T., & Jokat, W. (2011). Is there continental crust underneath the northern Natal Valley and the Mozambique Coastal Plains? *Geophysical Research Letters*, 38(14). <https://doi.org/10.1029/2011GL047659>
- Leinweber, V. T., & Jokat, W. (2012). The Jurassic history of the Africa-Antarctica corridor – New constraints from magnetic data on the conjugate continental margins. *Tectonophysics*, 530, 87–101. <https://doi.org/10.1016/j.tecto.2011.11.008>
- Leinweber, V. T., Klingelhoefer, F., Neben, S., Reichert, C., Aslanian, D., Matias, L., et al. (2013). The crustal structure of the Central Mozambique continental margin – Wide-angle seismic, gravity and magnetic study in the Mozambique Channel, Eastern Africa. *Tectonophysics*, 599, 170–196. <https://doi.org/10.1016/j.tecto.2013.04.015>
- Leprêtre, A., Klingelhoefer, F., Graindorge, D., Schnurle, P., Beslier, M. O., Yelles, K., et al. (2013). Multiphased tectonic evolution of the Central Algerian margin from combined wide-angle and reflection seismic data off Tipaza, Algeria. *Journal of Geophysical Research: Solid Earth*, 118(8), 3899–3916. <https://doi.org/10.1002/jgrb.50318>
- Leprêtre, A., Schnurle, P., Evain, M., Verrier, F., Moorcroft, D., De Clarens, P., et al. (2021). Deep structure of the North Natal Valley (Mozambique) using combined wide-angle and reflection seismic data. *Journal of Geophysical Research: Solid Earth*, 126(4), e2020JB021171. <https://doi.org/10.1029/2020JB021171>
- Loncke, L., Roest, W. R., Klingelhoefer, F., Basile, C., Graindorge, D., Heuret, A., et al. (2020). Transform marginal plateaus. *Earth-Science Reviews*, 203, 102940. <https://doi.org/10.1016/j.earscirev.2019.102940>
- Lorenzo, J. M. (1997). Sheared continent-ocean margins: An overview. *Geo-Marine Letters*, 17(1), 1–3. <https://doi.org/10.1007/PL00007201>
- Loureiro, A., Afilhado, A., Matias, L., Moulin, M., & Aslanian, D. (2016). Monte Carlo approach to assess the uncertainty of wide-angle layered models: Application to the Santos Basin, Brazil. *Tectonophysics*, 683, 286–307. <https://doi.org/10.1016/j.tecto.2016.05.040>
- Mahanjane, E. S. (2012). A geotectonic history of the northern Mozambique Basin including the Beira High – A contribution for the understanding of its development. *Marine and Petroleum Geology*, 36, 1–12. <https://doi.org/10.1016/j.marpetgeo.2012.05.007>
- Masclé, J., & Blarez, E. (1987). Evidence for transform margin evolution from the Ivory Coast–Ghana continental margin. *Nature*, 326(6111), 378–381. <https://doi.org/10.1038/326378a0>
- Melluso, L., Cucciniello, C., Petrone, C. M., Lustrino, M., Morra, V., Tiepolo, M., & Vasconcelos, L. (2008). Petrology of Karoo volcanic rocks in the southern Lebombo monocline, Mozambique. *Journal of African Earth Sciences*, 52(4–5), 139–151. <https://doi.org/10.1016/j.jafrearsci.2008.06.002>
- Mercier de Lépinay, M., Loncke, L., Basile, C., Roest, W. R., Patriat, M., Maillard, A., & de Clarens, P. (2016). Transform continental margins—Part 2: A worldwide review. *Tectonophysics*, 693, 96–115. <https://doi.org/10.1016/j.tecto.2016.05.038>
- Minshull, T. A., Lane, C. I., Collier, J. S., & Whitmarsh, R. B. (2008). The relationship between rifting and magmatism in the northeastern Arabian Sea. *Nature Geoscience*, 1(7), 463–467. <https://doi.org/10.1038/ngeo228>
- Momoh, E., Cannat, M., Watremez, L., Leroy, S., & Singh, S. C. (2017). Quasi-3-D seismic reflection imaging and wide-angle velocity structure of nearly amagmatic oceanic lithosphere at the ultraslow-spreading Southwest Indian Ridge. *Journal of Geophysical Research: Solid Earth*, 122(12), 9511–9533. <https://doi.org/10.1002/2017JB014754>
- Moulin, M., & Aslanian, D. (2016). PAMELA-MOZ03 cruise, RV Pourquoi pas? <https://doi.org/10.17600/16001600>
- Moulin, M., Aslanian, D., Evain, M., Leprêtre, A., Schnurle, P., Verrier, F., et al. (2020). Gondwana breakup, passive margin and contourite genesis: Messages from the Natal Valley. *Terra Nova*, 32, 205–214. <https://doi.org/10.1111/ter.12448>
- Moulin, M., & Evain, M. (2016). PAMELA-MOZ05 cruise, RV Pourquoi pas? <https://doi.org/10.17600/16009500>
- Mueller, C. O., & Jokat, W. (2017). Geophysical evidence for the crustal variation and distribution of magmatism along the central coast of Mozambique. *Tectonophysics*, 712–713, 1–703. <https://doi.org/10.1016/j.tecto.2017.06.007>
- Mueller, C. O., & Jokat, W. (2019). The initial Gondwana break-up – A synthesis based on new potential field data of the Africa-Antarctica Corridor. *Tectonophysics*, 750, 301–328. <https://doi.org/10.1016/j.tecto.2018.11.008>
- Mueller, C. O., Jokat, W., & Schreckenberger, B. (2016). The crustal structure of Beira High, central Mozambique – Combined investigation of wide-angle seismic and potential field data. *Tectonophysics*, 683, 233–254. <https://doi.org/10.1016/j.tecto.2016.06.028>
- Museur, T., Graindorge, D., Klingelhoefer, F., Roest, W. R., Basile, C., Loncke, L., & Sapin, F. (2021). Deep structure of the Demerara Plateau: From a volcanic margin to a Transform Marginal Plateau. *Tectonophysics*, 803, 228645. <https://doi.org/10.1016/j.tecto.2020.228645>
- Nemčok, M., Rybár, S., Sinha, S. T., Hermeston, S. A., & Ledvényiová, L. (2016). Transform margins: Development, controls and petroleum systems—an introduction. *Geological Society, London, Special Publications*, 431(1), 1–38. <https://doi.org/10.1144/SP431.15>
- Nguyen, L. C., Hall, S. A., Bird, D. E., & Ball, P. J. (2016). Reconstruction of the East Africa and Antarctica continental margins. *Journal of Geophysical Research Solid Earth*, 121, 4156–4179. <https://doi.org/10.1002/2015JB012776>
- Nonn, C., Leroy, S., Khanbari, K., & Ahmed, A. (2017). Tectono-sedimentary evolution of the eastern Gulf of Aden conjugate passive margins: Narrowness and asymmetry in oblique rifting context. *Tectonophysics*, 721, 322–348. <https://doi.org/10.1016/j.tecto.2017.09.024>
- O'Connor, J. M., Jokat, W., Regelous, M., Kuiper, K. F., Miggins, D. P., & Koppers, A. A. (2019). Superplume mantle tracked isotopically the length of Africa from the Indian Ocean to the Red Sea. *Nature Communications*, 10(1), 1–13. <https://doi.org/10.1038/s41467-019-13181-7>
- Parsieglá, N., Stankiewicz, J., Gohl, K., Ryberg, T., & Uenzelmann-Neben, G. (2009). Southern African continental margin: Dynamic processes of a transform margin. *Geochemistry, Geophysics, Geosystems*, 10(3). <https://doi.org/10.1029/2008GC002196>
- Peace, A. L., Phethean, J. J. J., Franke, D., Foulger, G. R., Schiffer, C., Welford, J. K., et al. (2019). A review of Pangaea dispersal and Large Igneous Provinces – In search of a causative mechanism. *Earth-Science Reviews*, 206, 102902. <https://doi.org/10.1016/j.earscirev.2019.102902>

- Péron-Pinvidic, G., & Manatschal, G. (2019). Rifted margins: State of the art and future challenges. *Frontiers of Earth Science*, 7, 218. <https://doi.org/10.3389/feart.2019.00218>
- Péron-Pinvidic, G., & Osmundsen, P. T. (2016). Architecture of the distal and outer domains of the Mid-Norwegian rifted margin: Insights from the Rån-Gjallar ridges system. *Marine and Petroleum Geology*, 77, 280–299. <https://doi.org/10.1016/j.marpetgeo.2016.06.014>
- Philippon, M., & Corti, G. (2016). Obliquity along plate boundaries. *Tectonophysics*, 693, 171–182. <https://doi.org/10.1016/j.tecto.2016.05.033>
- Ponte, J.-P., Robin, C., Guillocheau, F., Popescu, S., Suc, J.-P., Dall'Asta, M., et al. (2019). The Zambezi delta (Mozambique channel, East Africa): High resolution dating combining bio-orbital and seismic stratigraphy to determine climate (palaeoprecipitation) and tectonic controls on a passive margin. *Marine and Petroleum Geology*, 105, 293–312. <https://doi.org/10.1016/j.marpetgeo.2018.07.017>
- Raillard, S. (1990). *Les Marges de l'Afrique de l'Est et les Zones de Fracture Associées: Chaîne Davie et Ride du Mozambique* (p. 272). University Pierre et Marie Curie.
- Reeves, C. V., Teasdale, J. P., & Mahanjane, E. S. (2016). Insight into the Eastern Margin of Africa from a new tectonic model of the Indian Ocean. *Geological Society, London, Special Publications*, 431(1), 299–322. <https://doi.org/10.1144/SP431.12>
- Reuber, K. R., Pindell, J., & Horn, B. W. (2016). Demerara Rise, offshore Suriname: Magma-rich segment of the Central Atlantic Ocean, and conjugate to the Bahamas hot spot. *Interpretation*, 4(2), T141–T155. <https://doi.org/10.1190/INT-2014-0246.1>
- Ritzmann, O., Jokat, W., Czuba, W., Guterch, A., Mjelde, R., & Nishimura, Y. (2004). A deep seismic transect from Hovgård Ridge to northwestern Svalbard across the continental-ocean transition: A sheared margin study. *Geophysical Journal International*, 157(2), 683–702. <https://doi.org/10.1111/j.1365-246X.2004.02204.x>
- Roche, V., Leroy, S., Guillocheau, F., Revillon, S., Rufet, G., Watremez, L., et al. (2021). The Limpopo magma-rich transform margin (South Mozambique) – Part 2: Implications for the Gondwana breakup. *Tectonics*. <https://doi.org/10.1029/2021TC006914>
- Ryan, W. B., Carbotte, S. M., Coplan, J. O., O'Hara, S., Melkonian, A., Arko, R., et al. (2009). Global multi-resolution topography synthesis. *Geochemistry, Geophysics, Geosystems*, 10(3). <https://doi.org/10.1029/2008GC002332>
- Sage, F., Basile, C., Mascle, J., Pontoise, B., & Whitmarsh, R. B. (2000). Crustal structure of the continent–ocean transition off the Côte d'Ivoire–Ghana transform margin: Implications for thermal exchanges across the palaeotransform boundary. *Geophysical Journal International*, 143(3), 662–678. <https://doi.org/10.1046/j.1365-246X.2000.00276.x>
- Sahabi, M. (1993). *Un modèle général de d'évolution de l'océan indien* (Doctoral dissertation) (p. 383). Université de Bretagne Occidentale.
- Sallarès, V., Gailler, A., Gutscher, M. A., Graindorge, D., Bartolomé, R., Gracia, E., et al. (2011). Seismic evidence for the presence of Jurassic oceanic crust in the central Gulf of Cadiz (SW Iberian margin). *Earth and Planetary Science Letters*, 311(1–2), 112–123. <https://doi.org/10.1016/j.epsl.2011.09.003>
- Salman, G., & Abdula, I. (1995). Development of the Mozambique and Ruvuma sedimentary basins, offshore Mozambique. *Sedimentary Geology*, 96(1–2), 7–41. [https://doi.org/10.1016/0037-0738\(95\)00125-R](https://doi.org/10.1016/0037-0738(95)00125-R)
- Sandwell, D. T., & Smith, W. H. (2009). Global marine gravity from retracked Geosat and ERS-1 altimetry: Ridge segmentation versus spreading rate. *Journal of Geophysical Research: Solid Earth*, 114(B1). <https://doi.org/10.1029/2008JB006008>
- Sauter, D., Werner, P., Ceuleneer, G., Manatschal, G., Rospabé, M., Tugend, J., et al. (2021). Sub-axial deformation in oceanic lower crust: Insights from seismic reflection profiles in the Enderby Basin and comparison with the Oman ophiolite. *Earth and Planetary Science Letters*, 554, 116698. <https://doi.org/10.1016/j.epsl.2020.116698>
- Schimschal, C. M., & Jokat, W. (2018). The crustal structure of the continental margin east of the Falkland Islands. *Tectonophysics*, 724, 234–253. <https://doi.org/10.1016/j.tecto.2017.11.034>
- Senkans, A., Leroy, S., d'Acremont, E., Castilla, R., & Despinois, F. (2019). Polyphase rifting and break-up of the central Mozambique margin. *Marine and Petroleum Geology*, 100, 412–433. <https://doi.org/10.1016/j.marpetgeo.2018.10.035>
- Sinha, M. C., Loudon, K. E., & Parsons, B. (1981). The crustal structure of the Madagascar Ridge. *Geophysical Journal International*, 66(2), 351–377. <https://doi.org/10.1111/j.1365-246X.1981.tb05960.x>
- Stankiewicz, J., Parsiegla, N., Ryberg, T., Gohl, K., Weckmann, U., Trumbull, R., & Weber, M. (2008). Crustal structure of the southern margin of the African continent: Results from geophysical experiments. *Journal of Geophysical Research: Solid Earth*, 113(B10). <https://doi.org/10.1029/2008JB005612>
- Stockwell, J. W. (1999). The CWP/SU: Seismic Un* x package. *Computers & Geosciences*, 25, 415–419. [https://doi.org/10.1016/S0098-3004\(98\)00145-9](https://doi.org/10.1016/S0098-3004(98)00145-9)
- Sutra, E., Manatschal, G., Mohn, G., & Unternehr, P. (2013). Quantification and restoration of extensional deformation along the Western Iberia and Newfoundland rifted margins. *Geochemistry, Geophysics, Geosystems*, 14(8), 2575–2597. <https://doi.org/10.1002/ggge.20135>
- Svensen, H., Corfu, F., Polteau, S., Hammer, Ø., & Planke, S. (2012). Rapid magma emplacement in the Karoo Large Igneous Province. *Earth and Planetary Science Letters*, 325–326, 1–9. <https://doi.org/10.1016/j.epsl.2012.01.015>
- Thompson, G., Bryan, W. B., Frey, F. A., Dickey, J. S., & Davies, H. (1982). Petrology, geochemistry and original tectonic setting of basalts from the Mozambique Basin and Ridge (DSDP sites 248, 249 and 250), and from the Southwest Indian Ridge (DSDP site 251). *Marine Geology*, 48(3–4), 175–195. [https://doi.org/10.1016/0025-3227\(82\)90096-2](https://doi.org/10.1016/0025-3227(82)90096-2)
- Thompson, J. O., Moulin, M., Aslanian, D., De Clarens, P., & Guillocheau, F. (2019). New starting point for the Indian Ocean: Second phase of breakup for Gondwana. *Earth-Science Reviews*, 191, 26–56. <https://doi.org/10.1016/j.earscirev.2019.01.018>
- Torsvik, T. H., & Cocks, L. R. M. (2013). Gondwana from top to base in space and time. *Gondwana Research*, 24(3–4), 999–1030. <https://doi.org/10.1016/j.gr.2013.06.012>
- Torsvik, T. H., Smethurst, M. A., Burke, K., & Steinberger, B. (2006). Large igneous provinces generated from the margins of the large low-velocity provinces in the deep mantle. *Geophysical Journal International*, 167(3), 1447–1460. <https://doi.org/10.1111/j.1365-246X.2006.03158.x>
- Tréhu, A. M., Ballard, A., Dorman, L. M., Gettrust, J. F., Klitgord, K. D., & Schreiner, A. (1989). Structure of the lower crust beneath the Carolina Trough, US Atlantic continental margin. *Journal of Geophysical Research: Solid Earth*, 94(B8), 10585–10600. <https://doi.org/10.1029/JB094iB08p10585>
- Tsikalas, F., Eldholm, O., & Faleide, J. I. (2005). Crustal structure of the Lofoten–Vesterålen continental margin, off Norway. *Tectonophysics*, 404(3–4), 151–174. <https://doi.org/10.1016/j.tecto.2005.04.002>
- Vormann, M., Franke, D., & Jokat, W. (2020). The crustal structure of the southern Davie Ridge offshore northern Mozambique – A wide-angle seismic and potential field study. *Tectonophysics*, 778, 228370. <https://doi.org/10.1016/j.tecto.2020.228370>
- Watremez, L., Leroy, S., d'Acremont, E., Roche, V., Leprêtre, A., Verrier, F., et al. (2021). Deep-structure seismic imaging from the Limpopo magma-rich transform margin (South Mozambique). *SEANOE*. <https://doi.org/10.17882/76489>
- Watts, A. B. (2001). Gravity anomalies, flexure and crustal structure at the Mozambique rifted margin. *Marine and Petroleum Geology*, 18(4), 445–455. [https://doi.org/10.1016/S0264-8172\(00\)00079-9](https://doi.org/10.1016/S0264-8172(00)00079-9)
- Wessel, P., Smith, W. H., Scharroo, R., Luis, J., & Wobbe, F. (2013). Generic mapping tools: Improved version released. *Eos, Transactions American Geophysical Union*, 94(45), 409–410. <https://doi.org/10.1002/2013EO450001>

- White, R., & McKenzie, D. (1989). Magmatism at rift zones: The generation of volcanic continental margins and flood basalts. *Journal of Geophysical Research: Solid Earth*, 94(B6), 7685–7729. <https://doi.org/10.1029/JB094iB06p07685>
- White, R. S. (1992). Crustal structure and magmatism of North Atlantic continental margins. *Journal of the Geological Society*, 149(5), 841–854. <https://doi.org/10.1144/gsjgs.149.5.0841>
- White, R. S., McKenzie, D., & O'Nions, R. K. (1992). Oceanic crustal thickness from seismic measurements and rare earth element inversions. *Journal of Geophysical Research: Solid Earth*, 97(B13), 19683–19715. <https://doi.org/10.1029/92JB01749>
- Xu, W., Lithgow-Bertelloni, C., Stixrude, L., & Ritsema, J. (2008). The effect of bulk composition and temperature on mantle seismic structure. *Earth and Planetary Science Letters*, 275(1–2), 70–79. <https://doi.org/10.1016/j.epsl.2008.08.012>
- Zelt, C. A. (1999). Modelling strategies and model assessment for wide-angle seismic traveltimes data. *Geophysical Journal International*, 139(1), 183–204. <https://doi.org/10.1046/j.1365-246X.1999.00934.x>
- Zelt, C. A., & Forsyth, D. A. (1994). Modeling wide-angle seismic data for crustal structure: Southeastern Grenville Province. *Journal of Geophysical Research: Solid Earth*, 99(B6), 11687–11704. <https://doi.org/10.1029/93JB02764>
- Zelt, C. A., & Smith, R. B. (1992). Seismic traveltimes inversion for 2-D crustal velocity structure. *Geophysical Journal International*, 108(1), 16–34. <https://doi.org/10.1111/j.1365-246X.1992.tb00836.x>